A. Santana-Sánchez[1], L. Nikkanen[1], G. Toth[1], M. Ermakova[1,†], S. Kosourov[1], J. Walter[1,††], M. He[1,†††], E-M. Aro[1], Y. Allahverdiyeva[1]*

[1] Molecular Plant Biology, Department of Life Technologies, University of Turku, Turku FI-20014, Finland

[†] Present address: Research School of Biology, College of Medicine, Biology and Environment, Australian National University, Canberra ACT 2601, Australia.

[††] Present address: Department of Plant Sciences, University of Cambridge, Cambridge CB2 3EA, UK

[†††] Present address: Jiangsu Provincial Key Laboratory of Marine Biology, College of Resources and Environmental Sciences, Nanjing Agricultural University, Nanjing 210095, China

* Author for correspondence: allahve@utu.fi

Title: Flv3A facilitates O_2 photoreduction and affects H_2 photoproduction independently of Flv1A in diazotrophic *Anabaena* filaments

Short title: The role of vegetative-cell specific Flv1A and Flv3A in *Anabaena*

The author responsible for distribution of materials integral to the findings presented in this article in accordance with the policy described in the Instructions for Authors (https://academic.oup.com/plcell) is: Yagut Allahverdiyeva (allahve@utu.fi).

Abstract

The model heterocyst-forming filamentous cyanobacterium, *Anabaena* sp. PCC 7120 (*Anabaena*) represents multicellular organisms capable of simultaneously performing oxygenic photosynthesis in vegetative cells and the O_2-sensitive N_2-fixation inside the heterocysts. The flavodiiron proteins (FDPs) have been shown to participate in photoprotection of photosynthesis by driving excess electrons to O_2 (Mehler-like reaction). Here, we addressed the physiological relevance of the vegetative cell-specific Flv1A and Flv3A on the bioenergetic processes occurring in diazotrophic *Anabaena* under variable CO_2. We demonstrate that both Flv1A and Flv3A are required for proper induction of the Mehler-like reaction upon a sudden increase in light intensity, which is likely important for the activation of carbon-concentrating mechanisms (CCM) and CO_2 fixation. Under low CO_2 diazotrophic conditions, Flv3A is capable of mediating moderate O_2 photoreduction, independently of Flv1A, but in coordination with Flv2 and Flv4. Strikingly, the lack of Flv3A resulted in strong downregulation of the heterocyst-specific uptake hydrogenase, which led to enhanced H_2 photoproduction under both oxic and micro-oxic conditions. These results reveal a novel regulatory network between the Mehler-like reaction and the H_2 metabolism, which is of great interest for future photobiological production of H_2 in *Anabaena*.

Introduction

Filamentous heterocyst-forming cyanobacteria such as *Anabaena* sp. PCC 7120 (hereafter *Anabaena*) represent a unique group of prokaryotes capable of simultaneously performing two conflicting metabolic processes: (i) O_2-producing photosynthesis in vegetative cells; and (ii) O_2-sensitive N_2 fixation in heterocysts. This ability has evolved through cellular differentiation under nitrogen limiting growth conditions when some vegetative cells from the filament transform into specialized heterocyst cells that provide a microaerobic environment suitable for N_2 fixation. H_2 gas is naturally produced as an obligatory by-product of the N_2-fixation process carried out by nitrogenase, which is highly sensitive to O_2. The natural yield of H_2 gas production inside heterocysts is limited. This is due to rapid H_2 recycling, mainly by an uptake hydrogenase enzyme, which further returns electrons for the N_2-fixing metabolism (Tsygankov et al., 2007; Bothe et al., 2010).

In oxygenic photosynthesis, light drives the photosynthetic linear electron transport from water to NADPH, using Photosystem (PS) II, Cytochrome (Cyt) b_6f and PSI complexes embedded in the thylakoid membrane. These electron transport reactions are coupled to ATP synthesis *via* the generation of trans-thylakoid proton motive force (*pmf)*. The obtained NADPH and ATP are then used as reducing power for CO_2 fixation and cell metabolism. Environmental fluctuations in light and nutrient supply might result in the over-reduction of the photosynthetic machinery. Alleviation of excess electrons by the class-C Flavodiiron proteins (hereafter FDP) has been described in all oxygenic photosynthetic organisms, apart from angiosperms, red and brown algae (Helman et al., 2003; Zhang et al., 2009; Jokel et al., 2018; Gerotto et al., 2016; Chaux et al., 2017; Ilik et al., 2017; Alboresi et al., 2019; Shimakawa et al., 2021). This group of proteins act as strong electron outlets downstream of PSI by catalyzing the photoreduction of O_2 into H_2O (named the Mehler-like reaction) (Allahverdiyeva et al., 2013; 2015; Santana-Sánchez et al., 2019).

Six genes encoding FDPs have been reported in *Anabaena* (Ow et al., 2008; Zhang et al., 2009; Ermakova et al., 2013; Allahverdiyeva et al., 2015). Phylogenetic assessment has shown that four of these genes (*flv1A, flv3A, flv2*, and *flv4*) are highly similar to their homologs in *Synechocystis*. sp. PCC 6803 (hereafter *Synechocystis*), SynFlv1-SynFlv4. Recently, we demonstrated that SynFlv1 and SynFlv3 proteins function in coordination with, but distinctly from SynFlv2 and SynFlv4 (Santana-Sánchez et al., 2019). While the SynFlv1/Flv3 hetero-oligomer is mainly responsible for the initial fast and transient O_2

84 photoreduction during a sudden increase in light intensity, SynFlv2/Flv4 catalyzes steady O_2
85 photoreduction under illumination at air-level CO_2 (LC). Importantly, the single deletion of
86 any FDP strongly diminishes the O_2-photoreduction, indicating that O_2 photoreduction is
87 mainly catalyzed by the hetero-oligomeric forms working in an interdependent manner
88 (Santana-Sánchez et al., 2019; Nikkanen et al., 2020).

89 The two additional *Anabaena* FDP proteins, AnaFlv1B and AnaFlv3B, are exclusively
90 localized in the heterocysts (Ermakova et al., 2013). The AnaFlv3B protein was shown to
91 mediate the photoreduction of O_2 independently of AnaFlv1B, likely as a homo-oligomer,
92 playing an important role in maintaining micro-oxic conditions inside heterocysts under
93 illumination, which is crucial for N_2 fixation and H_2 production (Ermakova et al., 2014).
94 However, research on the role of heterocyst-specific AnaFlv1B and vegetative cell-specific
95 FDPs in diazotrophic cyanobacteria is still scarce.

96 Here, we addressed the physiological relevance of the AnaFlv1A and AnaFlv3A isoforms on
97 the bioenergetic processes occurring in vegetative cells and heterocysts of diazotrophic
98 *Anabaena*. AnaFlv1A and AnaFlv3A were shown to have a crucial photoprotective role
99 under fluctuating light intensities (FL), regardless of nitrogen or CO_2 availability, suggesting
100 functional analogy with homologs in *Synechocystis*. Importantly however, our results also
101 provided evidence for distinct functional roles of AnaFlv3A and AnaFlv1A. We showed that
102 by cooperating with AnaFlv2 and/or AnaFlv4, AnaFlv3A can function independently of
103 AnaFlv1A in O_2 photoreduction in low CO_2 conditions. AnaFlv3A was also indirectly linked
104 with the H_2 metabolism occurring inside heterocyst cells. Our work highlights the complex
105 regulatory network between oxygenic photosynthesis, nitrogen fixation and hydrogen
106 photoproduction.

107 **Results**

108 **Phenotypic characterization of *Anabaena* mutants deficient in Flv1A and Flv3A**

109 To investigate the function of the vegetative cell-specific Flv1A and Flv3A proteins in
110 diazotrophic *Anabaena* filaments, we used Δ*flv1A* and Δ*flv3A* deletion mutants
111 (Supplemental Figure 1 and Allahverdiyeva et al., 2013). Likewise, the SynFlv1 and
112 SynFlv3, the AnaFlv1A (encoded by *all3891*) and AnaFlv3A (encoded by *all3895*) proteins
113 are indispensable for diazotrophic and non-diazotrophic growth of *Anabaena* filaments under

114 severe fluctuating light intensities at both air level (low CO_2, LC) and 1-3 % CO_2 (high CO_2,
115 HC) (Supplemental Figures 2A and Allahverdiyeva et al., 2013).

116 Under constant light (at a photon flux density of 50 µmol photons m^{-2} s^{-1}), there were no
117 significant differences in the growth of these mutants compared to the WT, as measured by
118 OD_{750} (Supplemental Figure 2B) or concentration of chlorophyll *a* (Chl *a*). Total protein and
119 sugar content of the WT and Δ*flv1A* and Δ*flv3A* filaments were also similar (Table 1).

120 Light microscopic images of *Anabaena* filaments indicated that both Δ*flv1A* and Δ*flv3A*
121 mutants and WT had a similar ratio of vegetative cells to heterocysts (Table 1) and no visible
122 changes were observed in heterocyst morphology.

123 **Table 1. Growth characteristics and photosynthetic parameters of the WT, Δ*flv1A*, and**
124 **Δ*flv3A* filaments.** Experimental cultures were grown under diazotrophic LC conditions for 4
125 days. The maximum quantum yield of PSII (Fv/Fm), minimal level of fluorescence (Fo),
126 maximal fluorescence in the dark (F_m^D), maximal fluorescence (F_m'), quenching due to state
127 transition (qT). Values are means ± SD, n = 3-5 biological replicates. Asterisks indicate
128 statistically significant differences compared to the WT (t-test, $P < 0.05$).

Parameters	WT	Δ*flv1A*	Δ*flv3A*
OD_{750}	1.46±0.18	1.45±0.13	1.43±0.18
Chl *a*, µg mL^{-1}	7.01±0.80	6.66±0.76	6.97±0.96
Total protein, µg mL^{-1}	263.6±31.7	265.3±10.1	254±14.1
Total sugars, µg mL^{-1}	53.8±12.7	45.4±4.9	43.9±5.8
Heterocyst frequency (%)	12.7±1.1	12.1±0.9	10.7±2.1
Nitrogenase activity (C_2H_2 reduction), µmol mg $Chla^{-1}h^{-1}$	21.3±4.0	16.7±4.6	15.9±2.7*
F_v/F_m (with 10 µM DCMU)	0.45±0.05	0.5±0.01	0.49±0.01
F_o	0.91±0.01	0.86±0.00*	0.84±0.00*
F_m^D	1.39±0.02	1.25±0.02*	1.26±0.01*
F_m' (SP 1)	1.46±0.05	1.42±0.04	1.49±0.04
qT	0.05±0.02	0.14±0.01*	0.18±0.01*

129 **Fluorescence and P700 oxidoreduction properties of Δ*flv1A* and Δ*flv3A***

Diazotrophic *Anabaena* WT, Δ*flv1A*, and Δ*flv3A* filaments, grown under LC and HC, were next subjected to fluorescence analyses under growth light intensity to disclose the impact of Flv1A and Flv3A, common or specific, on photosynthetic electron transport. The dark-adapted WT filaments showed a relatively low maximal fluorescence in the dark (F_m^D) (state 2). Upon exposure to actinic light intensity, maximal fluorescence (F_m') slightly increased, indicating a transition of filaments to state 1 (Figure 1A). The state 2-to-state 1 transition observed upon illumination was less pronounced in HC-grown WT filaments (Figure 1B). The effective yield of PSII [Y(II)], calculated for each saturating pulse (SP), remained stable (0.34±0.02 - 0.30±0.01) during the illumination of WT filaments grown both under LC (Figure 1C) and HC (Figure 1D) conditions.

Both the Δ*flv1A* and Δ*flv3A* mutants showed significantly lower F_m^D than WT in LC (Figure 1 and Table 1), implying a more pronounced state 2 in the dark. Accordingly, a stronger state 2-to-state 1 transition (qT in Table 1) was observed during illumination in comparison to WT, similarly to the phenotype previously described in the *Synechocystis* Δ*flv3* mutant (Elanskaya et al., 2021). Notably, during the dark-to-light transition, the fluorescence kinetics were differently affected in the two mutants grown under LC conditions. Illumination of Δ*flv3A* filaments resulted in a rapid increase of the fluorescence level which was gradually quenched but remained at a higher steady-state level (F_s) compared to WT and the Δ*flv1A* mutant. The Δ*flv1A* mutant showed only a moderate increase and then a gradual decay of fluorescence, reaching the WT F_s level after 4 min of illumination. Differently from LC grown filaments, the Δ*flv1A* and Δ*flv3A* mutants grown under HC conditions revealed a similar fluorescence increase during the dark-to-light transition, which gradually decayed and reached the WT levels by the end of the illumination period (Figure 1B).

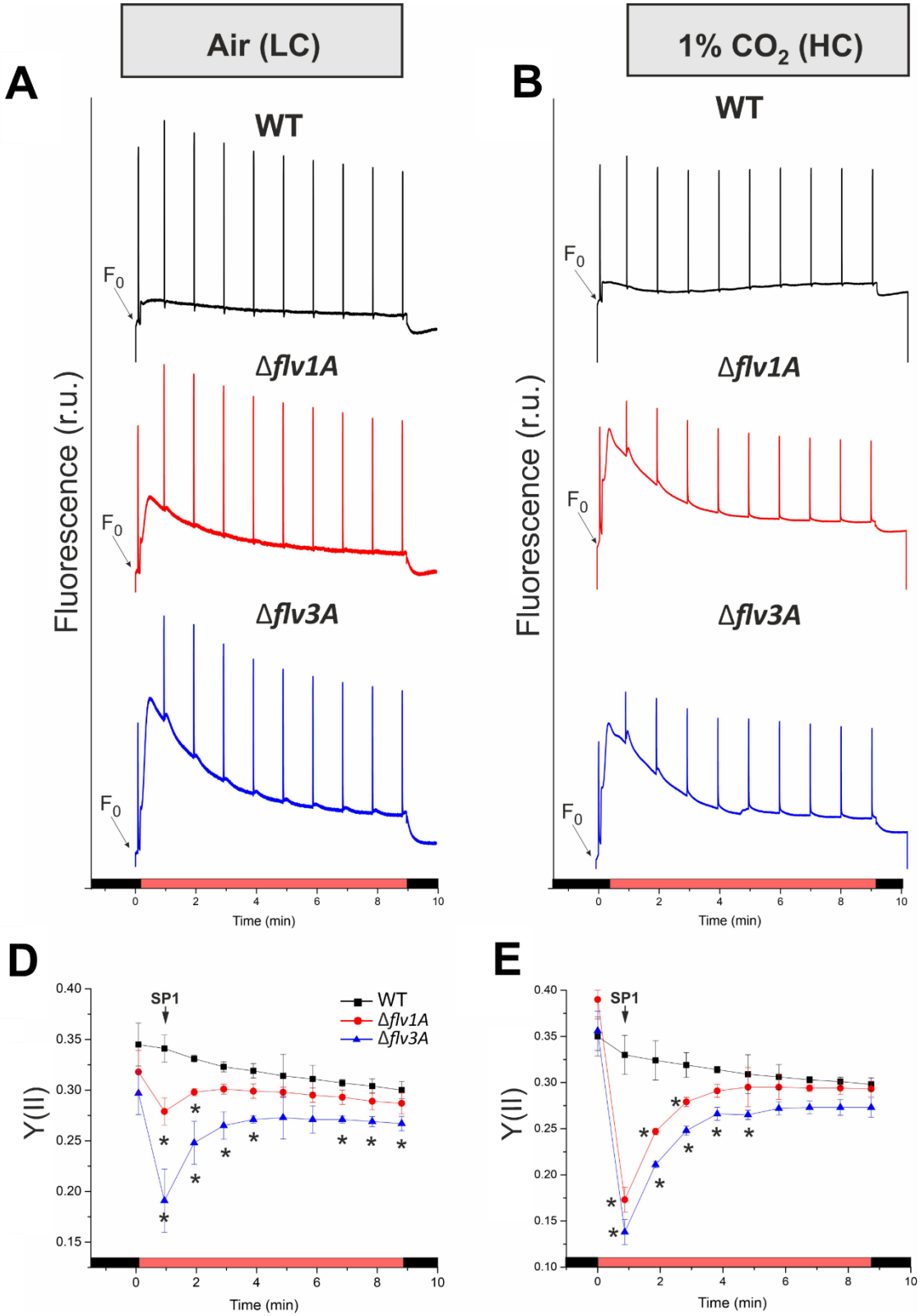

Figure 1. Fluorescence analysis of the diazotrophic *Anabaena* WT, Δ*flv1A*, and Δ*flv3A*. (A, C) Filaments were cultivated under air (LC) or (B, D) under air supplemented with 1% CO_2 (HC). Representative traces of 3 biological replicates are shown (A, B). Cells were dark acclimated for 10 min before illumination with 50 µmol photons m^{-2} s^{-1} of actinic light. The effective yield of PSII [Y(II)] was calculated by applying saturating pulses during induction curve measurements (C, D). Values are means ± SD, n = 3 biological replicates. Asterisks indicate statistically significant differences compared to the WT (t-test, $P < 0.05$). r.u., relative units.

153

The effective yield of PSII, Y(II) echoed high fluorescence levels and small variable fluorescence (F_v') upon illumination by SP1, showing a strong drop both in LC- (84% and 62% that of WT in Δ*flv1A* and Δ*flv3A* mutants, respectively) and HC-grown filaments (53% and 39% that of WT in Δ*flv1A* and Δ*flv3A* mutants, respectively) (Figure 1C, D). After that, the Y(II) values gradually recovered over the course of illumination, though Δ*flv3A* did not reach the WT levels (Figure 1C). Notably, the maximum quantum yield of PSII, F_v/F_m, did not differ significantly between the mutants and the WT (Table 1).

Examination of the transient post-illumination increase of fluorescence level (F_0 rise), which reflects the NDH-1 mediated reduction of the PQ pool in darkness (Mi et al., 1995), demonstrated a notably higher F_0 rise in both Δ*flv1A* and Δ*flv3A* mutants grown under LC and HC conditions (Supplemental Figure 3A, B). In line with the lower F_m^D (Table 1), this finding suggests elevated electron flux into the PQ pool in the Δ*flv1A* and Δ*flv3A* mutants, presumably mediated by NDH-1, in comparison to WT. Considering that the abundance of NdhK, the core subunit of the NDH-1 complex, was similar between all genotypes (Supplemental Figure 4D) the difference in F_0 rise is likely caused by higher availability of reduced ferredoxin (Fd), the likely electron donor to both FDPs and NDH-1 (Nikkanen et al., 2021), or by post-translational regulatory factors.

At the onset of high irradiance both the Δ*flv1* (Supplemental Figure 5) and Δ*flv3* mutants of *Synechocystis* are unable to rapidly re-oxidize Fd, causing accumulation of electrons at P700 (Nikkanen et al., 2020; Theune et al., 2021). To determine whether this occurs in the *Anabaena* Δ*flv1A* and Δ*flv3A* mutants, we determined the high light-induced fast redox changes of Fd and P700 from near-infrared absorbance differences using the Dual KLAS/NIR spectrophotometer. The results indicated that similarly to *Synechocystis* Δ*flv3* (Nikkanen et al., 2020) and Δ*flv1* mutants (Supplemental Figure 5), both *Anabaena* mutants also suffered from delayed re-oxidation of Fd and P700 upon illumination, and showed slower post-illumination re-oxidation of Fd (Figure 2). Unlike in the *Synechocystis* mutants, there was a clear difference between the Δ*flv1A* and Δ*flv3A* mutants of *Anabaena*, with the Δ*flv3A* strain displaying more severe delay in re-oxidation of Fd and P700 than Δ*flv1A*.

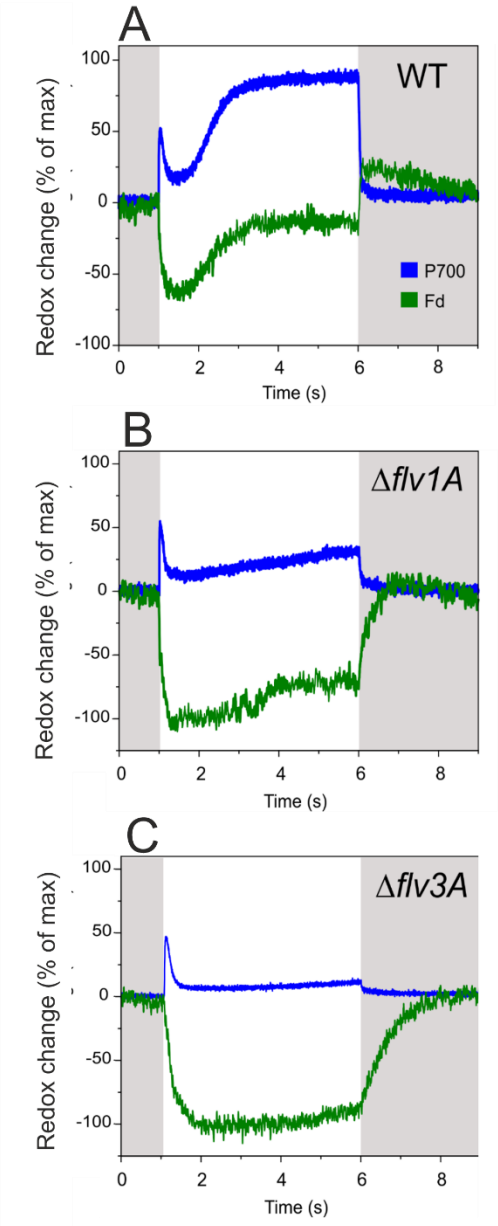

Figure 2. Redox changes of P700 and Fd upon dark-light-dark transitions in the diazotrophic *Anabaena* WT, Δ*flv1A*, and Δ*flv3A* filaments. The cells were grown under 50 µmol photons m^{-2} s^{-1} and air-level CO_2 (LC) for 4 days, harvested and adjusted to Chl *a* concentration of 20 µg mL^{-1}. Cells were dark-adapted for 10 min, after which absorbance differences of four near-infrared wavelength pairs were measured with the Dual KLAS/NIR spectrophotometer during 5 s actinic illumination at 503 µmol photons m^{-2} s^{-1} and subsequent darkness. P700 and Fd redox changes were then deconvoluted from the absorbance differences using specifically determined differential model plots (model spectra) for *Anabaena* (see Materials and methods). Maximal levels of Fd reduction and P700 oxidation in each sample were used to normalize the traces. Representative traces of 3 biological replicates are shown.

182

Real-time gas exchanges in *Anabaena* FDP mutants

To clarify the specific impacts of *flv1A* and *flv3A* deletions on real-time gas fluxes in the diazotrophic filaments of *Anabaena*, we used membrane inlet mass spectrometry (MIMS) analysis (Figure 3). The MIMS technique combined with the use of $^{18}O_2$ isotopologue allows distinguishing between light-induced O_2 reduction (uptake) and photosynthetic O_2 production. The net O_2 evolution rate was calculated as the difference between the rates of gross O_2 evolution and O_2 uptake in the light. For all MIMS measurements, gas exchange was monitored for 4 min in dark followed by 5 min of high irradiance (500 µmol photons m^{-2} s^{-1}) and for an additional 3 min in the dark.

192

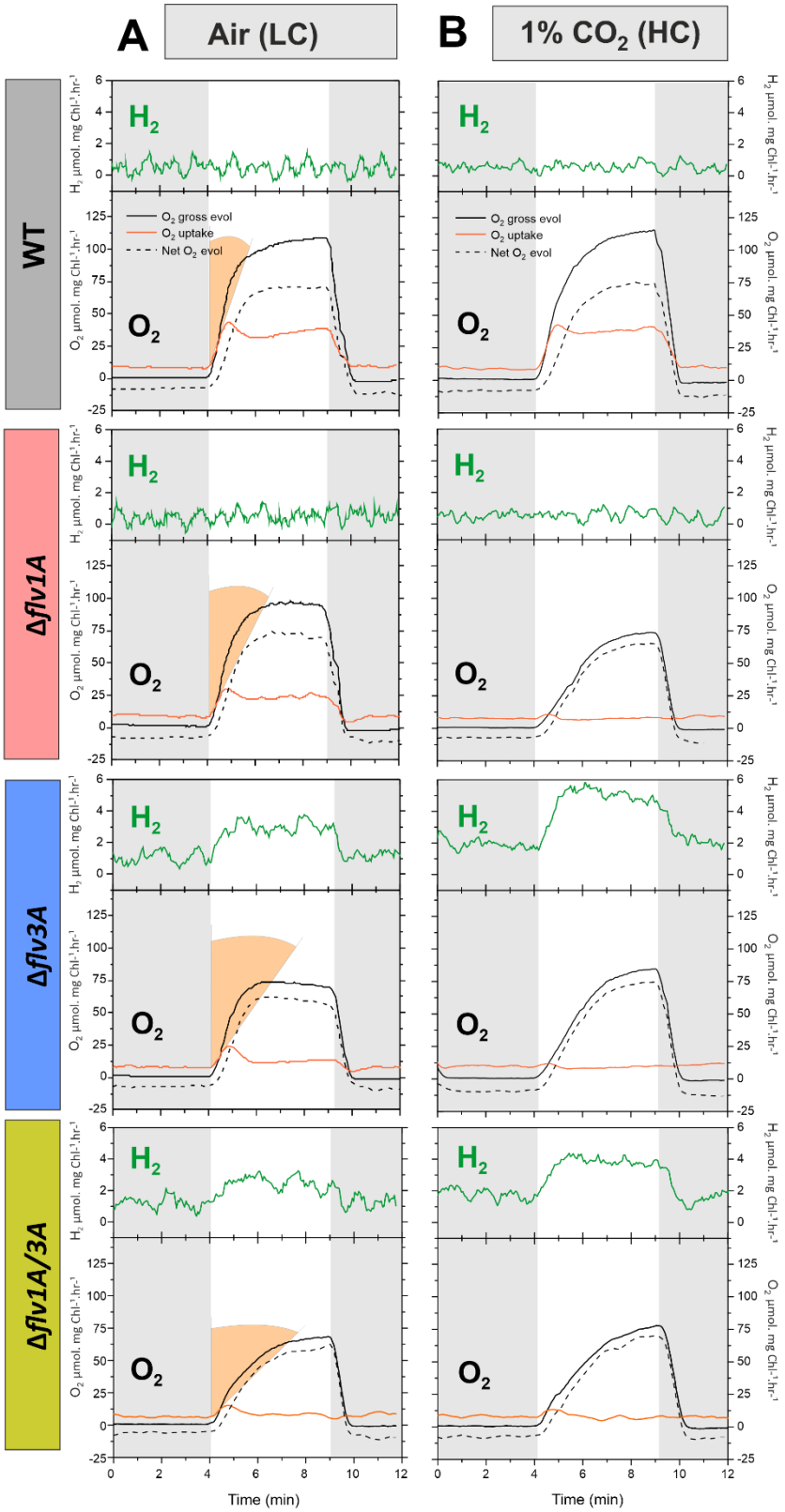

Figure 3. O_2 and H_2 exchange rates of the diazotrophic *Anabaena* WT, Δ*flv1A* and Δ*flv3A* filaments. The filaments were cultivated for 4 days under air (LC) (A) and high carbon (1% CO_2 in the air, HC) (B), after which the filaments were harvested and the Chl *a* concentration adjusted to 10 µg mL^{-1}. Gas exchange rates were calculated in darkness (grey areas of the graphs) and under illumination with actinic white light at 500 µmol photons m^{-2} s^{-1}. For LC measurements, samples were supplemented with 1.5 mM $NaHCO_3$. Orange shading indicates the differences in the initial slope of the O_2 photoreduction rates. The plots are representative of three independent biological replicates.

Illumination of WT filaments grown under LC demonstrated a rapid increase in the rate of O_2 uptake from 10.6±2.7 µmol O_2 mg Chl a^{-1} h^{-1} in darkness to 34.6±0.2 µmol O_2 mg Chl a^{-1} h^{-1} in light. This fast induction phase was followed by a decay that stabilized at 28.4±1.4 µmol O_2 mg Chl a^{-1} h^{-1} after 3 min (Figure 3A, Supplemental Table 1). This pattern resembles, to some extent, previously described triphasic kinetics of O_2 photoreduction in *Synechocystis* grown under LC conditions (Santana-Sánchez et al., 2019), and in HC-grown *Chlamydomonas reinhardtii* cells illuminated with high light intensity (Saroussi et al., 2019). Both mutants showed slightly lower O_2 uptake rates in darkness than the WT (Supplemental Table 1) but the rate of O_2 consumption under illumination was affected to different extents in Δ*flv1A* and Δ*flv3A* filaments. The Δ*flv3A* mutant exhibited strong impairment of light-induced O_2 uptake, showing a maximal rate of 15.6±0.1 µmol O_2 mg Chl a^{-1} h^{-1} (52 % lower than the WT) at the onset of light, which declined to a residual rate of 4.3±0.2 µmol O_2 mg Chl a^{-1} h^{-1} by the end of illumination. In contrast to the *Synechocystis* Δ*flv1* mutant (Supplemental Figure 7) where O_2 reduction is almost fully eliminated, the *Anabaena* Δ*flv1A* filaments showed an intermediate phenotype whereby a maximum light-induced O_2 reduction rate of 22.2±2.8 µmol O_2 mg Chl a^{-1} h^{-1} (34% lower than WT) was observed, which declined to 15.5±1.2 µmol O_2 mg Chl a^{-1} h^{-1} (Figure 3A). Moreover, both Δ*flv1A* and Δ*flv3A* mutants showed slower activation of O_2 photoreduction, with a more pronounced lag-phase in Δ*flv3A* (Figure 3A, orange shading). These results suggested that both AnaFlv1A and AnaFlv3A contribute to the Mehler-like reaction, but to a differing extent and presumably in different homo/hetero-oligomeric arrangements.

To clarify whether the homo-oligomers of AnaFlv1A in Δ*flv3A* and conversely, the homo-oligomers of AnaFlv3A in Δ*flv1A* mutants contribute to the observed O_2 photoreduction rates (Figure 3A), we constructed a double mutant Δ*flv1A*/Δ*flv3A* (Supplemental Figure 6). MIMS analysis revealed that concomitant inactivation of both *flv1A* and *flv3A* strongly inhibited the O_2 photoreduction in *Anabaena* filaments cultivated under LC conditions (Figure 3A) suggesting either contribution of AnaFlv1 and AnaFlv3 homo-oligomers to O_2 photoreduction in the single mutants or involvement of AnaFlv2 and/or AnaFlv4 proteins in this process. Previous studies with *Synechocystis* cells (Zhang et al., 2009; Wang et al., 2004; Eisenhut et al., 2012; Santana-Sánchez et al., 2019) and non-diazotrophic *Anabaena* WT filaments (Ermakova et al., 2013) demonstrated high transcript abundance of *flv2* and *flv4* at LC. Therefore, we next investigated the abundance of *flv2* and *flv4* transcripts in diazotrophic *Anabaena* filaments grown under LC and HC using RT-qPCR. The Δ*flv1A* and Δ*flv3A*

mutants grown under LC demonstrated significantly higher *flv2* and *flv4* transcript levels compared to the WT (Supplemental Figure 4A). Under HC, transcript abundances of *flv2* and *flv4* did not differ between the mutants and the WT but were drastically lower in all genotypes compared to LC conditions (Supplemental Figure 4B). This prompted us to examine the possible contribution of AnaFlv2 and AnaFlv4 proteins to the Mehler-like reaction by comparing the O_2 photoreduction rates in Δ*flv1A* and Δ*flv3A* mutants grown under LC (Figure 3A) *vs* HC conditions (Figure 3B), where the expression of *flv2* and *flv4* were found to be induced and repressed, respectively.

While the O_2 photoreduction in WT filaments grown under HC was comparable to that under LC conditions (Figure 3A), the inactivation of *flv1A* and/or *flv3A* fully eliminated light-induced O_2 reduction in the filaments grown under HC (Figure 3B). This result suggests that the highly expressed *flv2* and *flv4* likely contribute to O_2 photoreduction in diazotrophic Δ*flv1A* and Δ*flv3A* filaments grown under LC conditions. Nevertheless, further elucidation is needed to verify the functioning of the AnaFlv2/Flv4 hetero-oligomer or different FDP oligomer compositions in O_2 photoreduction.

It is important to note that under LC conditions, while gross O_2 evolution and net photosynthetic O_2 production rates of the Δ*flv1A* mutant were comparable to those of the WT, the Δ*flv3A* mutant demonstrated lower gross and net O_2 evolution rates (Figure 3A, Supplemental Table 1). Strikingly, the initial peak in CO_2 uptake rates associated with the CCM activation (Liran et al., 2018) as well as the steady-state of CO_2 fixation of both deletion mutants were significantly diminished compared to the WT, and the Δ*flv3A* strain showed pronounced impairment than Δ*flv1A* (Supplemental Table 1, Supplemental Figure 8B). Under HC conditions, both mutants had lower gross O_2 evolution (65.9±7.3 and 76.8±6.5 μmol O_2 mg Chl a^{-1} h^{-1}, respectively) relative to the WT (122.2±14.8 μmol O_2 mg Chl a^{-1} h^{-1}) and a delay in the induction of O_2 evolution upon illumination (Figure 3B). Accordingly, the activation of CO_2 fixation under HC conditions was slower and decreased in both mutants compared to WT (Supplemental Figure 8C). In the Δ*flv1A*/Δ*flv3A* double mutant a delay in gross O_2 evolution was observed under LC that was more severe than in Δ*flv3A* cells (Figure 3A), while under HC all three mutant strains were similarly impaired (Figure 3B). This suggests that not only AnaFlv3A, but also AnaFlv1A may be performing some AnaFlv2-4-dependent but AnaFlv3A-independent function in LC that affects photosynthetic electron transport.

Consequences of *flv1A* or *flv3A* deletion on diazotrophic metabolism

Based on the results above it is clear that AnaFlv1A and AnaFlv3A impact the photosynthetic apparatus to different extents in LC-grown diazotrophic *Anabaena*. In comparison to the inactivation of AnaFlv1A, the deletion of AnaFlv3A resulted in a stronger reduction of the PQ pool, leading to a consistent decrease of PSII effective yield (Figure 1C) and, eventually, lower net O_2 evolution rates over the illumination period (Figure 3A). On the other hand, previous studies with different diazotrophic *Anabaena* species have demonstrated that the disruption of PSII activity in vegetative cells has implications for N_2 and H_2 metabolism inside heterocysts, thus, modulating the diazotrophic metabolism of filaments (Khetkorn et al., 2012; Chen et al., 2014). We, therefore, examined whether the absence of AnaFlv1A or AnaFlv3A from vegetative cells has a long-distance impact on the heterocyst metabolism. To this end, we analyzed the nitrogenase activity and H_2 fluxes of diazotrophic *Anabaena* WT, Δ*flv1A* and Δ*flv3A* mutants.

As demonstrated in Table 1, both Δ*flv1A* and Δ*flv3A* mutants showed somewhat lower nitrogenase activity in comparison to WT filaments, yet only the nitrogenase activity of the Δ*flv3A* mutant was significantly lower compared to WT. Real-time gas exchange monitored by MIMS (Figure 3) revealed no changes in the H_2 gas concentration in WT and Δ*flv1A* during the dark-light transition. In contrast, the Δ*flv3A* mutant showed an increase in H_2 level in the dark and a clear light-induced H_2 gas production (1.7±0.4 µmol mg Chl a^{-1} h^{-1}) (Figure 3A). This result was confirmed by a second independent Δ*flv3A* mutant strain showing similar light-induced H_2 production (Δ*flv3A*_C2 in Supplemental Figure 8A). Interestingly, the Δ*flv3A* mutant cultivated under HC conditions demonstrated an even higher H_2 photoproduction rate (2.8±0.8 µmol mg Chl a^{-1} h^{-1}, Figure 3B). Although Δ*flv3A* filaments showed real-time H_2 production under oxic conditions, the rate of H_2 production remained low.

Next, we monitored H_2 in anoxic cultures using a Clark-type electrode. Under the N_2 atmosphere, the Δ*flv3A* mutant demonstrated a significantly higher yield of H_2 photoproduction accompanied by a three times higher specific H_2 production rate compared to the WT (Figure 4A, Supplemental Figure 9A). To confirm that the observed H_2 production is nitrogenase-mediated, we monitored the reaction under an argon (Ar) atmosphere as it is known that in the absence of N_2 substrate, nitrogenase reduces protons to H_2 (Hoffman et al., 2014). Indeed, the specific H_2 photoproduction rate of the WT filaments under an Ar was

about 7-fold higher compared to the N_2 atmosphere (Supplemental Figure 9A). In the case of Δ*flv3A*, the yield of H_2 photoproduction was strongly enhanced under an Ar and the production rate increased by around 10 times compared to N_2 (Supplemental Figure 9A). In addition, a drastically decreased transcript abundance of *hoxH* in both Δ*flv1A* and Δ*flv3A* mutants compared to the WT (Supplemental Figure 9B), implied a negligible contribution of Hox to H_2 production in Δ*flv3A* mutant. Collectively, these results provide evidence that the enhanced H_2 production in the Δ*flv3A* mutant is mediated by nitrogenase.

However, the observed decrease in nitrogenase activity (Table 1) did not correlate with an increase in H_2 photoproduction in Δ*flv3A* (Figure 3A). It is well known that the net nitrogenase-mediated production of H_2 in heterocysts is strongly affected by the activity of uptake hydrogenase (Hup), which oxidizes H_2 (Tamagnini et al., 2007). Therefore, it is conceivable that the impairment of the Hup function would account for the increased production of H_2 in Δ*flv3A*. To examine the H_2 fluxes, we traced the uptake of Deuterium ($^2H_2$, D_2) by the WT, Δ*flv1A*, and Δ*flv3A*. Whilst WT and Δ*flv1A* filaments efficiently consumed D_2, Δ*flv3A* showed a significantly lower capacity for D_2 uptake (Figure 4B). These observations confirmed that the impaired capacity of the Δ*flv3A* mutant to recycle H_2 could be the reason for the increased accumulation of H_2 observed in Δ*flv3A* mutant.

To better understand the molecular mechanism behind the defective H_2 uptake of Δ*flv3A*, we analyzed the transcript and protein abundances of the large subunit of Hup (HupL). We found significant downregulation of the mature form of *hupL* transcript in both Δ*flv1A* and Δ*flv3A* mutants, in comparison to the WT (Figure 4C). Importantly, *hupL* transcript level in Δ*flv3A* was significantly lower than in the Δ*flv1A* mutant. Immunoblotting with specific antibody further revealed the lack of detectable HupL protein in Δ*flv3A*, a result comparable to the *hupL*-disrupted mutant (Δ*hupL*), while the Δ*flv1A* mutant showed only a lowered level of HupL relative to the WT (Figure 4D). Taken together, these results demonstrate that the lack of HupL protein in heterocyst cells of Δ*flv3A* is the reason behind the enhanced nitrogenase based H_2 photoproduction observed for this mutant.

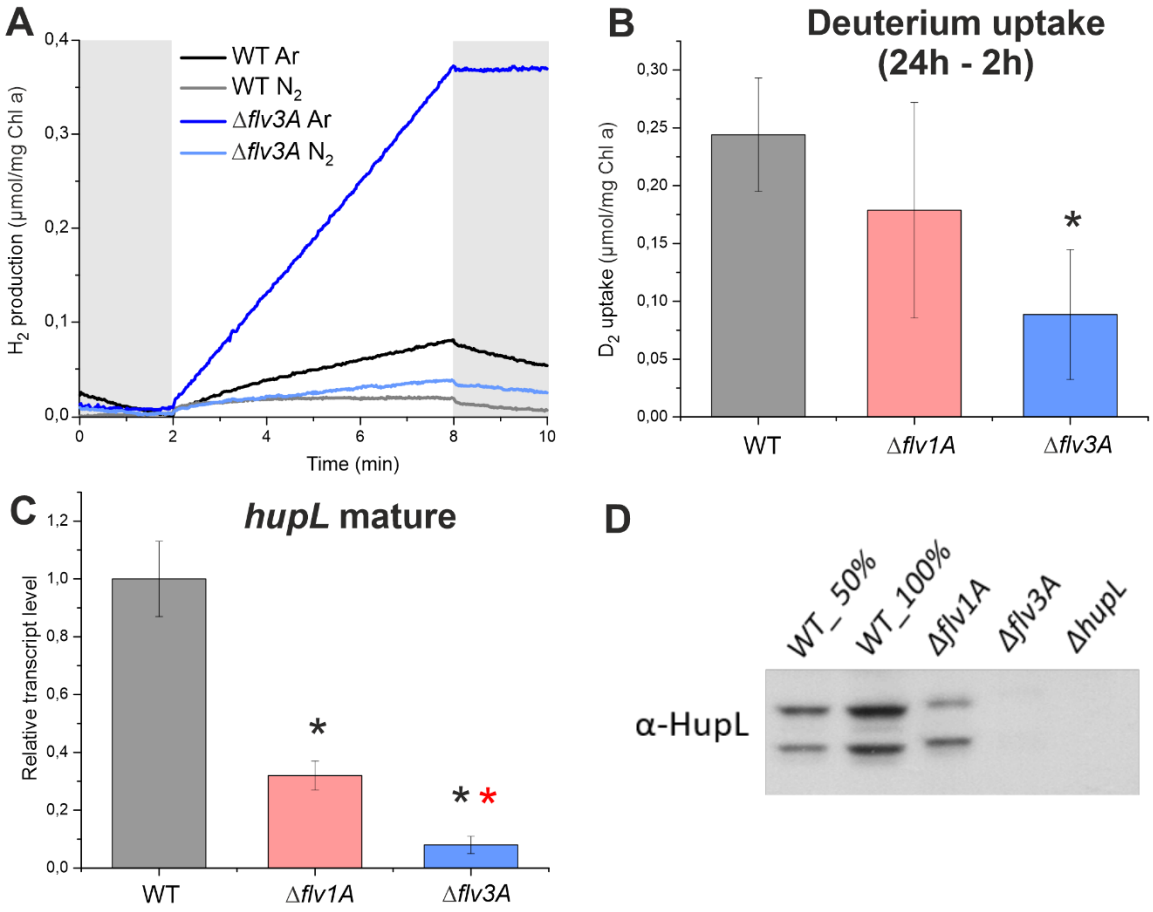

Figure 4. H_2 metabolism of diazotrophic filaments of *Anabaena* WT, Δ*flv1A*, and Δ*flv3A*. (A) H_2 production yield was monitored by a H_2 electrode under an Ar or N_2 atmosphere in the dark (grey areas) and under 800 µmol photons m^{-2} s^{-1} light. (B) Deuterium uptake by the filaments was calculated from the difference in D_2 concentration between 2 h and 24 h after the injection in the vials initially flushed with Ar. (C) Relative transcript level of the mature *hupL*. (D) Immunodetection of HupL with a specific antibody. (E) Nitrogenase activity was measured using the acetylene reduction assay. Values are Mean ± SD, n = 3 biological replicates. Black asterisk indicates statistically significant differences compared to the WT (t-test, $P < 0.05$). Red asterisk indicates statistically significant differences compared to the Δ*flv1A* mutant (t-test, $P < 0.05$).

Discussion

The heterocyst-forming cyanobacteria are considered one of the earliest forms of multicellular filaments in the history of life (Schirrmeister et al., 2016). Despite the extensive characterization of heterocyst differentiation, little is known about the co-regulation and interdependence of the two contrasting processes of N_2 fixation and oxygenic photosynthesis occurring in heterocysts and vegetative cells, respectively. Under challenging environmental conditions, diazotrophic cyanobacteria must find an optimal balance between photochemical reactions and downstream processes that consume electrons in both cell types. In this work, we employed Δ*flv1A* and Δ*flv3A* mutants of *Anabaena* to examine the physiological

significance of the vegetative cell-specific AnaFlv1A and AnaFlv3A proteins on the bioenergetic processes of diazotrophic cyanobacteria. Our results provide evidence that, in contrast to the *Synechocystis* homolog, AnaFlv3A can mediate moderate O_2 photoreduction independently of AnaFlv1A and in coordination with AnaFlv2 and AnaFlv4 under LC conditions. Moreover, the vegetative-cell specific AnaFlv3A protein exhibits important link to the H_2 metabolism inside the heterocyst, since the inactivation of this protein results in high H_2 photoproduction even under ambient air. Nevertheless, we have demonstrated that both AnaFlv1A and AnaFlv3A proteins, presumably as hetero-oligomers, are required for efficient induction of the Mehler-like reaction during dark-to-light transitions, are crucial for photoprotection when light intensity rapidly fluctuates, and are likely needed for the activation of CO_2 assimilation.

In the absence of AnaFlv1A, AnaFlv3A can team up with AnaFlv2 and/or AnaFlv4 to mediate O_2 photoreduction under LC conditions

In line with previous transcriptional analysis showing a decrease in the expression of both *flv1A* and *flv3A* in *Anabaena* WT upon the shift to diazotrophic conditions (Ermakova et al. 2014), the single deletions of AnaFlv1A or AnaFlv3A did not affect the diazotrophic growth of mutants under continuous illumination compared to the WT (Table 1). However, both AnaFlv1A and AnaFlv3A proteins are indispensable during sudden changes in light intensity, similar to their homologous proteins in other species (Supplemental Figure 1A, Allahverdiyeva et al., 2013; Gerotto et al., 2016; Jokel et al., 2018). Here, we have demonstrated that when both AnaFlv1A and AnaFlv3A proteins are expressed in WT filaments, the rate of the Mehler-like reaction is rapidly increased during the dark-to-light transition likely due to the activity of the AnaFlv1A/Flv3A hetero-oligomer (Figure 3). Accordingly, the absence of either AnaFlv1A or AnaFlv3A delays rise in O_2 photoreduction (Figure 3A) resulting in over-reduction of the PQ pool upon illumination (Figure 1A), causing a decrease in PSII yield (Figure 1C) and impairment of PSI and Fd oxidation (Figure 2). This phenotype is aggravated in the mutant lacking AnaFlv3A, which showed a stronger state 2-to-state 1 transition and more severe inability to oxidize PSI than the mutant lacking AnaFlv1A (Figure 1 and Figure 2). Differently from the *Synechocystis* Δ*flv1* mutant (Supplemental Figure 7), AnaFlv3A can promote O_2 photoreduction in the *Anabaena* Δ*flv1A* mutant (Figure 3A), resulting in only about 45% inhibition of steady-state O_2 photoreduction and 35% decrease in Y(II) in *Anabaena* under LC growth conditions (Supplemental Table 1).

The near elimination of the steady-state O_2 photoreduction in the Δ*flv1A/flv3A* double mutant under LC and the single mutants under HC conditions (where AnaFlv2 and AnaFlv4 are strongly downregulated) supports (i) functional AnaFlv3A/Flv2-4 oligomerization, and/or (ii) cooperation between the AnaFlv3A/Flv3A homo-oligomer and AnaFlv2/Flv4 hetero-oligomers. Accordingly, the strong impairment of O_2 photoreduction in Δ*flv3A* might be due to the inability of AnaFlv1A to function as a homo-oligomer and/or cooperate with AnaFlv2/Flv4. It is worth emphasizing that both Δ*flv1A* and Δ*flv3A* mutants showed similarly enhanced accumulation of *flv2* and *flv4* transcripts (Supplemental Figure 4A). While the Δ*flv1A* mutant displayed WT-like *flv3A* transcript and protein levels, the Δ*flv3A* mutant showed an elevated *flv1A* transcript level compared to the WT (Supplemental Figure 4C). This shows that the inhibition of O_2 photoreduction in Δ*flv3A* is not due to the downregulation of other FDPs. No contribution of the SynFlv3/Flv3 homo-oligomer in the Mehler-like reaction was observed *in vivo* (Mustila et al., 2016), contrary to previous *in vitro* studies suggesting a function of SynFlv3/Flv3 homo-oligomers in NAD(P)H-dependent O_2 reduction (Vicente et al., 2002, Brown et al., 2019). Instead, a possible photoprotective function of SynFlv3/Flv3 homo-oligomers *via* an unknown electron transport network was proposed (Mustila et al., 2016). In *Anabaena* Δ*flv1A* mutant, AnaFlv3A/Flv3A homo-oligomers may, for example, be involved in controlling the cation homeostasis, which in turn may affect the reversible association of AnaFlv2/Flv4 hetero-oligomers with the thylakoid membrane, and consequently, their involvement in O_2 photoreduction. It is also important to note that the oligomer formation scenario in the mutants might be different in *Anabaena* WT filaments. Overall, the obtained results suggest an important role for AnaFlv3A, but not AnaFlv1A, in mediating steady-state O_2 photoreduction under diazotrophic LC conditions in an AnaFlv2/Flv4-dependent. Moreover, in LC but not in HC conditions, the lack of both AnaFlv1A and AnaFlv3A resulted in a more severe delay in induction of O_2 evolution during dark-to-light transition in comparison to the lack of AnaFlv3A only (Figure 3). This suggests that AnaFlv1A may also function in coordination with AnaFlv2/4 independently of Flv3A in an unknown role that facilitates photosynthetic electron transport. Understanding the exact functions of AnaFlv2 and/or AnaFlv4 in these processes and their interactions with AnaFlv1A and AnaFlv3A requires further investigation.

Even though AnaFlv1A and AnaFlv3A contribute to the Mehler-like reaction to different extents, both Δ*flv1A* and Δ*flv3A* mutants exhibited reduced CCM activity, as deduced from lowered initial peaks in CO_2 uptake rate during dark-to-light transition and reduction of

steady-state CO_2 uptake in comparison to WT (Supplemental Figure 8B, Supplemental Table 1). This is likely to result from impaired energization of CCM in the absence of AnaFlv1A or AnaFlv3A. SynFlv1 and SynFlv3 have been shown to have a crucial role in the generation of *pmf* during the dark-to-light transition (Nikkanen et al., 2020), comparable to that of FLVA/B in *P. patens* (Gerotto et al., 2016) and *C. reinhardtii* (Chaux et al., 2017). Moreover, the *pmf* generated by FDPs and CET has been recently shown to be important for inducing and maintaining CCM activity in *C. reinhardtii* (Burlacot et al., 2021). We hypothesize that AnaFlv1A/Flv3A hetero-oligomer is required to rapidly induce the Mehler-like reaction, likely being important for the generation of *pmf* and possibly for induction of CCM activity during the dark-to-light transition. The molecular mechanism of the FDP-dependency of the CCM requires further investigation however, as the mechanisms of CCM differ between *Chlamydomonas* and cyanobacteria (Price et al 2008). Moreover, in *Synechocystis* mutants lacking Flv1/3 *pmf* generation during the first minute of dark-to-light transitions is severely impaired, CCM induction is largely unaffected at least in standard conditions (Nikkanen et al., 2020). In *Anabaena* however, both Δ*flv1A* and Δ*flv3A* strains demonstrated impaired induction of CCM (Supplemental Figure 8B), suggesting that *Anabaena* may differ from *Synechocystis* in the extent to which CCM induction is *pmf*-dependent.

Compelling evidence has recently been provided for dynamic coordination and functional redundancy between NDH-1 and SynFlv1/Flv3, jointly contributing to efficient oxidation of PSI in *Synechocystis* (Nikkanen et al., 2020) and in *Physcomitrella patens* (Storti et al., 2020a, 2020b). NDH-1-mediated cyclic electron transport (CET) in *Anabaena* could also partially compensate for a lack of AnaFlv1A and AnaFlv3A as evidenced by a stronger F_0 rise observed in both mutants (Supplemental Figure 3A). Unlike *Synechocystis* cells, *Anabaena* filaments express orthologs of plastid terminal oxidase (PTOX, *all2096*) (McDonald et al., 2003). It has been proposed that in *C. reinhardtii* and vascular plants, PTOX functions as an electron valve directing electrons from plastoquinol to O_2, thereby controlling the redox state of the PQ pool (Stepien and Johnson, 2018, Saroussi et al., 2019; Nawrocki et al., 2019) and being involved in diverse metabolic processes such as the regulation of CET, state transition and carotenoid biosynthesis (Nawrocki et al., 2019). We cannot exclude possible contribution of PTOX to the residual O_2 photoreduction observed in the Δ*flv3A* mutant (Figure 3A), and/or as a sensor of the redox state of the PQ pool and regulator of NDH-dependent CET, thus limiting electron pressure on the acceptor-side of PSI (Bolte et al., 2020).

425

426 **Inactivation of AnaFlv3A leads to enhanced nitrogenase-based H_2 photoproduction**
427 **under oxic conditions**

428 Demonstration of elevated photoproduction of H_2 gas in diazotrophic filaments lacking
429 vegetative cell-specific AnaFlv3A under oxic and microoxic conditions (Figure 4) provided
430 intriguing information about bioenergetic interdependence between vegetative cells and
431 heterocysts. The heterocyst-originated production of H_2 in the Δ*flv3A* mutant was rapidly
432 induced upon exposing the filaments to light and occurred concomitantly with the evolution
433 of O_2 in neighbouring vegetative cells (Figure 3). Moreover, the rate of H_2 photoproduction
434 in the Δ*flv3A* mutant responded positively to an increase in CO_2 availability (Figure 3B).

435 In the absence of N_2, the main substrate for nitrogenase, all electrons can be directed to H_2
436 production (Hoffman et al., 2014) allowing a less costly reaction, whereby only 4 moles of
437 ATP are required to produce one mole of H_2. In this work, the removal of N_2 substrate (by
438 replacement with Ar) led to a 10-fold increase of H_2 photoproduction rate in Δ*flv3A*,
439 demonstrating the occurrence of nitrogenase-dependent H_2 photoproduction in this mutant
440 (Figure 4A). A recent report suggested that overexpressing Flv3B lead to more stable
441 microoxic conditions inside the heterocysts, notably increasing the H_2 production yield,
442 presumably *via* the bidirectional hydrogenase Hox (Roumezi et al., 2020). In contrast to the
443 unidirectional production of H_2 by nitrogenase, Hox catalyzes the reversible reduction of
444 protons to H_2 (Bothe et al., 2010). We do not consider the contribution of Hox to the
445 photoproduction of H_2 by the Δ*flv3A* mutant, as the net production does not fit with the
446 bidirectional nature of the enzyme. Moreover, significant downregulation in the Δ*flv3A*
447 mutant of transcripts from *hoxH*, encoding one of the subunits (Supplemental Figure 9B)
448 further supports this assumption. Altogether, these results indicate that the increased light-
449 induced H_2 photoreduction of the Δ*flv3A* mutant is mediated by nitrogenase activity.

450 Strikingly, it turned out that the increase in H_2 photoproduction yield in the Δ*flv3A* mutant
451 was due to significant downregulation of HupL, the large subunit of the uptake hydrogenase,
452 evidenced both at the transcript and protein levels (Figure 4C, 4D). The absence of functional
453 Hup suppressed the H_2 recycling pathway (Figure 4B) and caused the release of H_2,
454 photoproduced by nitrogenase, from the heterocysts of Δ*flv3A* filaments (Figure 3, Figure
455 4A). Thereby, our results highlight a regulatory network between the two metabolic processes

in different compartments: The Flv3A-mediated metabolic processes in the vegetative cells and the H_2 metabolism in the heterocysts. It is likely that the redox state of the PQ pool in vegetative cells, affected by the activity of Flv3A, has a regulatory role on the H_2 metabolism in heterocysts. However, the nature of the molecular signal from reduced PQ that ultimately regulates gene expression in heterocysts remains unknown. The redox state of the PQ pool in likely correlates with the availability of soluble reducing cofactors in the cytosol of vegetative cells, and while evidence in *Anabaena* is lacking, those cofactors may be interchanged between vegetative cells and heterocysts, inducing changes in metabolism and gene expression. A majority of the NADPH needed for the nitrogen metabolism in heterocysts is understood to be derived from the oxidative pentose phosphate pathway breaking down carbohydrates imported from vegetative cells, (Cumino et al., 2007) but it is plausible that more direct exchange of cofactors also occurs, analogously to the malate redox shuttle between cytosol and the chloroplast in plants and algae. Nevertheless, the molecular mechanism underlying this regulatory network between different cell types needs further elucidation.

Taken together, our results demonstrate that similarly to SynFlv1 and SynFlv3, both vegetative-cells specific AnaFlv1A and AnaFlv3A are indispensable under harsh FL conditions regardless of nitrogen or CO_2 availability, most likely maintaining sufficient oxidation of the photosynthetic electron transport chain by catalysing the Mehler-like reaction as AnaFlv1A/Flv3A hetero-oligomers. Under LC, AnaFlv3A is able to perform moderate O_2 photoreduction in coordination with AnaFlv2 and AnaFlv4 proteins and independently of AnaFlv1A. AnaFlv3A may either stimulate the activity of AnaFlv2/Flv4 hetero-oligomers indirectly via an unknown function, or participate in forming functional hetero-oligomers with AnaFlv2 and Flv4. The deletion of AnaFlv3A was concomitant with the downregulation of the heterocyst-specific Hup enzyme resulting in increased bioproduction of H_2. This novel regulatory network between the metabolisms of carbon and nitrogen as well as response to oxidative stress in diazotrophic *Anabaena*, might represent an unexploited source for the future of biotechnological applications.

Materials and Methods

Strains and culture conditions

Anabaena sp. PCC 7120 strain was used as the wild-type (WT) in this study. The Δ*flv1A* and Δ*flv3A* mutants (Allahverdiyeva et al., 2013) and the Δ*hupL* mutant (Masukawa et al., 2002) were previously reported. For construction of the double mutant Δ*flv1A/flv3A*, the BamHI-XbaI region of the mutated *flv1A* construct was replaced with the spectinomycin/streptomycin resistance cassette. The generated plasmid was transferred into Δ*flv3A* and sucrose, neomycin, and spectinomycin was used for selection. Segregation of the mutants was verified by PCR. Culture stocks of Δ*flv1A* and Δ*flv3A* mutants were maintained in BG-11 medium supplemented with 40 μg mL^{-1} neomycin, while the Δ*hupL* mutant was supplemented with 20 μg mL^{-1} spectinomycin.

Pre-cultures were grown in Z8x medium (lacking combined nitrogen, pH 7.0-7.3, Kotai, 1972) at 30 °C and under constant white light of 75 μmol photons m^{-2} s^{-1} without antibiotics. For this, the filaments were inoculated at OD_{750}= 0.1 in 200 mL Z8x medium (in 500 mL flasks) and were continuously bubbled with air (0.04% CO_2, LC) or with air supplemented with 1% CO_2 (HC) if not specifically mentioned. Pre-cultures were harvested at the logarithmic growth phase, inoculated at OD_{750}= 0.1 in fresh Z8x medium and experimental cultures were grown under similar pre-experimental conditions (75 μmol photons m^{-2} s^{-1} illumination and bubbling with air or 1% CO_2 supplemented). For all physiological measurements and transcription profiling, experimental cultures were harvested after 4 days of growth and experiments were conducted in 3-5 independent biological replicates.

Determination of heterocyst frequency

Alcian blue was used to stain the polysaccharide layer of the heterocyst envelope. Cell suspensions were mixed (1:8) with a solution of 0.5% Alcian Blue stain in 50% ethanol-water. Stained samples were visualized using a Wetzlar light microscope (Leitz) and x400 magnification micrographs were taken. Around 1000-2000 cells were counted per sample, and the heterocyst frequency was determined as a percentage of total cells counted.

Viability analysis

For viability analysis, pre-cultures were grown in BG-11o under air supplemented with 3% CO_2 and serial dilutions of cell suspension, from OD_{750} 1.0 until 10^{-3}, were prepared. From each dilution, 5 μL were dropped on solid BG-11o (without combined nitrogen) agar plates. The plates were cultivated for 4 days under ambient air or air supplemented with 3% CO_2.

MIMS measurements

In vivo measurements of $^{16}O_2$ (m/z = 32), $^{18}O_2$ (m/z = 36), CO_2 (m/z = 44) and H_2 (m/z = 2) fluxes were monitored using a membrane inlet mass spectrometry (MIMS) as described previously (Mustila et al., 2016). Harvested filaments were resuspended with fresh Z8x medium, adjusted to Chl *a* 10 µg mL^{-1} and acclimated for 1 hr to the growth conditions. For LC samples, the concentration of dissolved total inorganic carbon was saturated with 1.5 mM $NaHCO_3$ before the measurement.

To measure Deuterium uptake, the filaments were flushed with Ar inside gas-tight vials for 15 min, then 1.2 mL pure D_2 (2 % in headspace) was injected into each vial. Changes of D_2 in the gas phase were measured at 2 h and 24 h after D_2 addition. 250 µL gas sample from the headspace of the vials was injected into the MIMS chamber. The calibration of D_2 concentration was performed by injecting known concentrations of D_2 into the media.

Fluorescence analysis

A pulse amplitude modulated fluorometer Dual-PAM-100 (Walz) was used to monitor Chl *a* fluorescence and P700 absorbance, independently. Harvested filaments were resuspended in fresh Z8x medium to the Chl *a* concentration of 15 µg mL^{-1} and then kept for about 1 hr under the growth conditions. Before the measurements, samples were dark-adapted for 10 min. The measurement started with a saturating pulse in darkness to determine F_m^D. Then, the samples were illuminated with red actinic light at a photon flux density of 50 µmol photons m^{-2} s^{-1} for 380 s whilst saturating pulses (5000 µmol photons m^{-2} s^{-1}, 400 ms) were given every minute (SP1-SP9). Photosynthetic parameters were determined as described previously (Huokko et al 2017).

Determination of P700 and Fd redox changes from near-infrared absorbance

The absorbance differences at 780–820 nm, 820–870 nm, 840–965 nm and 870–965 nm were measured with the Dual KLAS/NIR spectrophotometer (Walz). Redox change kinetics of P700 and Fd were deconvoluted from the four difference signals using differential model plots (model spectra) (Supplemental Figure 10) that were measured for *Anabaena* using protocols described earlier (Theune et al., 2021) with the modification for the Fd model spectrum, we used the Δ*flv1A*/Δ*flv3A* mutant instead of anoxic conditions to impair the Mehler-like reaction (see Figure 2) and to sufficiently slow down the re-oxidation Fd. For

P700 and plastocyanin (PC) model spectra, we used WT *Anabaena* filaments. Due to low signal quality, the PC traces were omitted from Figure 2. As noted for *Synechocystis* earlier (Theune et al., 2021), it is likely that the redox kinetics of P700 and PC in *Anabaena* may be closely related, thus making it difficult to extract a PC signal of large magnitude.

Experimental cultures, as well as cultures used for determination of the model spectra, were grown at 50 µmol photons m^{-2} s^{-1} and under air-level CO_2 (LC) in Z8x medium for 4 days, then adjusted to *Chl* a concentration of 20 µg mL^{-1} by reinoculating pelleted cells in fresh medium. Cells were dark-adapted for 10 min, after which absorbance differences of the four wavelength pairs were measured during 5 s actinic illumination at 500 µmol photons m^{-2} s^{-1} and subsequent dark. The maximal levels of P700 oxidation and Fd reduction were determined for each sample by utilizing the NIRMAX script (Klughammer and Schreiber 2016), and the obtained experimental deconvoluted traces were then normalized to the maximal values. The Dual-KLAS/NIR measurement of *Synechocystis* Δ*flv1* cells was performed as described previously (Nikkanen et al., 2020).

H_2 measurement by Clark-type electrode

H_2 concentration was monitored under anaerobic conditions using a Clark-type Pt-Ag/AgCl electrode chamber (DW1/AD, Hansatech) connected to a homemade polarographic box. Experimental cultures were harvested, resuspended in fresh Z8x medium and adjusted to the Chl *a* concentration of about 3-4 µg mL^{-1}. The resulting suspensions (~30 mL) were transferred into 75 mL glass vials, sealed and sparged with either nitrogen (N_2) or argon (Ar) for 30 min in the dark to achieve anaerobic conditions. Then, cultures were incubated under the corresponding atmosphere for another 2 h in the dark at 25 ^{o}C. 4 mL of dark-adapted suspension were transferred into the chamber with an anaerobic gas-tight syringe and H_2 concentration was monitored during 6 min illumination with actinic light of 800 µmol photons m^{-2} s^{-1} after which the light was switched off. The H_2 production rates were calculated using linear regression.

Nitrogenase activity essay

Acetylene reduction assay was used to determine nitrogenase activity as described previously (Leino et al. 2014). 5 mL of experimental samples were transferred into 23 mL vials, flushed with argon for 20 min and supplemented with 10% acetylene in the headspace. Vials were

kept for 20 hr under 50 µmol photons m^{-2} s^{-1} at 30 °C with gentle agitation (120 rpm). After this, 20 µL of gas sample was withdrawn from the headspace of the vial and analysed for ethylene content using a gas chromatograph equipped with Carboxen®-1010 PLOT Capillary Column and FID detector. The enzyme activity was calculated from the peak area and normalised to the total protein content.

Chl *a* and total sugar determination

Chl *a* was extracted from cells in 90% methanol and the concentration was determined by measuring absorbance at 665 nm and multiplying it with the extinction coefficient factor 12.7 (Meeks & Castenholz, 1971). For total sugar determination, 1 mL of experimental samples were collected, washed and diluted to 1:1 with MQ-water before the sugar measurement. Total sugar content was obtained using the colourimetric method described earlier (DuBois et al., 1956).

Protein extraction and immunoblotting

Total protein extracts were isolated as described previously (Zhang et al., 2009). Electrophoresis and immunoblotting were performed according to an earlier report (Mustila et al., 2016). Protein-specific antibodies raised against Flv3A (Agrisera), PsaB (AS10 695, Agrisera), NdhK (Agrisera), and HupL (kindly provided by P. Tamagnini) were used in this study.

RNA isolation and RT-qPCR analysis

Isolation of total RNA, reverse transcription and qPCR analysis was performed as described earlier (Ermakova et al., 2013). *rnpB gene* was used as a reference for normalization. The primer pairs used in this study are listed in Table 3.

Table 2. Oligonucleotide sequences used for qPCR.

Gene name	Forward primer (5′ →3′)	Reverse primer (3′ →5′)
flv2 (*all4444*)	cgacttttgcccaaacttta	gatcgccatcataattcctg
flv4 (*all4446*)	ctgctattcgctgtttggat	ttcactaagccgctatggtc
hupL_mature	agtagccgcttctacgatga	acccaaccacacaggttcta
hoxH	gggacaaatcctccaatccc	tttgctcctcccaacacttc

rnpB	ggactaggggttggggact	acgagggcgattatctatctg

Acknowledgements

We thank Prof. Paula Tamagnini for the HupL antibody.

Funding

This work was supported by the NordForsk Nordic Center of Excellence "NordAqua" (no. 82845 to Y.A.), the Academy of Finland (project no. 315119 to Y.A).

Authors contribution: Y.A. conceived the study, A.S-S., G.T., M.E., L.N, S.K., and Y.A. designed the research. A.S-S. performed most of the experiments. M.E. performed growth characterization of the mutants. L.N. performed KLAS-NIR, S.K measured H_2 production using the electrode. M.H. performed Deuterium uptake experiment. G.T performed RT-qPCR experiments and J.W constructed an independent Δ*flv3A* mutant. A.S.S. drafted the manuscript and all authors revised and approved it.

List of supplemental data

- Supplemental Figure 1. Title. The genomic structure of *Anabaena* Δf*lv1A* and Δ*flv3A* mutants used in this work.
- Supplemental Figure 2. Title. Growth characterization of WT, Δ*flv1A* and Δ*flv3A* filaments.
- Supplemental Figure 3. Title. F0 rise of Anabaena WT, Δ*flv1A* and Δ*flv3A*.
- Supplemental Figure 4. Title. Analyses of transcript and protein abundance in the diazotrophic WT, Δ*flv1A* and Δ*flv3A* filaments.
- Supplemental Figure 5. DUAL-KLAS-NIR kinetics of P700, PC and Fd in *Synechocystis* Δ*flv1* mutant.
- Supplemental Figure 6. Title. Fluorescence induction curves of diazotrophic *Anabaena* Δ*flv1A/3A* cultivated under LC or HC.
- Supplemental Figure 7. Title. O_2 exchange rates of the non-diazotrophic *Synechocystis* Δflv1 mutant.

- Supplemental Figure 8. Title. Gas exchange analysis of the diazotrophic *Anabaena* filaments.
- Supplemental Figure 9. Title. H_2 metabolism in diazotrophic filaments of *Anabaena* WT and FDP mutants.
- Supplemental Figure 10. Title. Differential model blots (DMPs) for deconvolution of PC, P700, and Fd signals with the DUAL-KLAS-NIR spectrometer
- Supplemental Table 1. Title. Rates of CO_2 and O_2 exchange in WT, Δ*flv1A*, and Δ*flv3A* filaments grown under air (LC) or in the air supplemented with 1% CO_2 (HC).

References

Allahverdiyeva, Y., Ermakova, M., Eisenhut, M., Zhang, P., Richaud, P., Hagemann, M., ... & Aro, E. M. (2011). Interplay between flavodiiron proteins and photorespiration in *Synechocystis* sp. PCC 6803. *Journal of Biological Chemistry*, *286*(27), 24007-24014.

Allahverdiyeva, Y., Mustila, H., Ermakova, M., Bersanini, L., Richaud, P., Ajlani, G., ... & Aro, E. M. (2013). Flavodiiron proteins Flv1 and Flv3 enable cyanobacterial growth and photosynthesis under fluctuating light. *Proceedings of the National Academy of Sciences*, *110*(10), 4111-4116.

Allahverdiyeva, Y., Isojärvi, J., Zhang, P., & Aro, E. M. (2015). Cyanobacterial oxygenic photosynthesis is protected by flavodiiron proteins. *Life*, *5*(1), 716-743.

Bailey, S., Melis, A., Mackey, K. R., Cardol, P., Finazzi, G., van Dijken, G., ... & Grossman, A. (2008). Alternative photosynthetic electron flow to oxygen in marine *Synechococcus*. Biochimica et Biophysica Acta (BBA)-Bioenergetics, 1777(3), 269-276.

Bolte, S., Marcon, E., Jaunario, M., Moyet, L., Paternostre, M., Kuntz, M., & Krieger-Liszkay, A. (2020). Dynamics of the localization of the plastid terminal oxidase inside the chloroplast. Journal of Experimental Botany, 71(9), 2661-2669.

Bothe, H., Schmitz, O., Yates, M. G., & Newton, W. E. (2010). Nitrogen fixation and hydrogen metabolism in cyanobacteria. *Microbiology and molecular biology reviews*, *74*(4), 529-551.

654 Braakman, R., Follows, M. J., & Chisholm, S. W. (2017). Metabolic evolution and the self-
655 organization of ecosystems. Proceedings of the National Academy of Sciences, 114(15),
656 E3091-E3100.

657 Brown, K. A., Guo, Z., Tokmina-Lukaszewska, M., Scott, L. W., Lubner, C. E., Smolinski,
658 S., ... & King, P. W. (2019). The oxygen reduction reaction catalyzed by *Synechocystis*
659 sp. PCC 6803 flavodiiron proteins. Sustainable Energy & Fuels, 3(11), 3191-3200.

660 Cai, Y., & Wolk, C. P. (1997). *Anabaena* sp. strain PCC 7120 responds to nitrogen
661 deprivation with a cascade-like sequence of transcriptional activations. Journal of
662 Bacteriology, 179(1), 267-271.

663 Chaux, F., Burlacot, A., Mekhalfi, M., Auroy, P., Blangy, S., Richaud, P., & Peltier, G.
664 (2017). Flavodiiron proteins promote fast and transient O_2 photoreduction in
665 Chlamydomonas. Plant physiology, 174(3), 1825-1836.

666 Chen, M., Li, J., Zhang, L., Chang, S., Liu, C., Wang, J., & Li, S. (2014). Auto-flotation of
667 heterocyst enables the efficient production of renewable energy in cyanobacteria.
668 Scientific reports, 4(1), 1-9.

669 Cumino, A.C., Marcozzi, C., Barreiro, R., & Salerno, G.L. Carbon cycling in Anabaena sp.
670 PCC 7120. Sucrose synthesis in the heterocysts and possible role in nitrogen fixation.
671 Plant Physiology, 143, 1385–1397.

672 Daley, S. M., Kappell, A. D., Carrick, M. J., & Burnap, R. L. (2012). Regulation of the
673 cyanobacterial CO 2-concentrating mechanism involves internal sensing of NADP+ and
674 α-ketogutarate levels by transcription factor CcmR. PLoS One, 7(7), e41286.

675 Eisenhut, M., Georg, J., Klähn, S., Sakurai, I., Mustila, H., Zhang, P., ... & Aro, E. M.
676 (2012). The antisense RNA As1_flv4 in the cyanobacterium Synechocystis sp. PCC 6803
677 prevents premature expression of the flv4-2 operon upon shift in inorganic carbon supply.
678 *Journal of Biological Chemistry*, *287*(40), 33153-33162.

679 Elanskaya, I. V., Bulychev, A. A., Lukashev, E. P., & Muronets, E. M. (2021). Deficiency
680 in flavodiiron protein Flv3 promotes cyclic electron flow and state transition under high
681 light in the cyanobacterium *Synechocystis* sp. PCC 6803. *Biochimica et Biophysica Acta*
682 *(BBA)-Bioenergetics*, *1862*(1), 148318.

683 Ermakova, M., Battchikova, N., Richaud, P., Leino, H., Kosourov, S., Isojärvi, J., ... & Aro,
684 E. M. (2014). Heterocyst-specific flavodiiron protein Flv3B enables oxic diazotrophic
685 growth of the filamentous cyanobacterium Anabaena sp. PCC 7120. *Proceedings of the*
686 *National Academy of Sciences*, *111*(30), 11205-11210.

687 Ermakova, M., Battchikova, N., Allahverdiyeva, Y., & Aro, E. M. (2013). Novel
688 heterocyst-specific flavodiiron proteins in *Anabaena* sp. PCC 7120. *FEBS letters*, *587*(1),
689 82-87.

690 Flaherty, B. L., Van Nieuwerburgh, F., Head, S. R., & Golden, J. W. (2011). Directional
691 RNA deep sequencing sheds new light on the transcriptional response of Anabaena sp.
692 strain PCC 7120 to combined-nitrogen deprivation. BMC genomics, 12(1), 1-10.

693 Forchhammer, K., & Selim, K. A. (2020). Carbon/nitrogen homeostasis control in
694 cyanobacteria. FEMS microbiology reviews, 44(1), 33-53.

695 Gerotto, C., Alboresi, A., Meneghesso, A., Jokel, M., Suorsa, M., Aro, E. M., &
696 Morosinotto, T. (2016). Flavodiiron proteins act as safety valve for electrons in
697 Physcomitrella patens. Proceedings of the National Academy of Sciences, 113(43),
698 12322-12327.

699 González, A., Bes, M. T., Valladares, A., Peleato, M. L., & Fillat, M. F. (2012). FurA is the
700 master regulator of iron homeostasis and modulates the expression of tetrapyrrole
701 biosynthesis genes in A nabaena sp. PCC 7120. Environmental microbiology, 14(12),
702 3175-3187.

703 González, A., Angarica, V. E., Sancho, J., & Fillat, M. F. (2014). The FurA regulon in
704 *Anabaena* sp. PCC 7120: in silico prediction and experimental validation of novel target
705 genes. Nucleic Acids Research, 42(8), 4833-4846.

706 Guío, J., Sarasa-Buisan, C., Velázquez-Campoy, A., Bes, M. T., Fillat, M. F., Peleato, M.
707 L., & Sevilla, E. (2020). 2-oxoglutarate modulates the affinity of FurA for the ntcA
708 promoter in *Anabaena* sp. PCC 7120. FEBS letters, 594(2), 278-289.

709 Hackenberg, C., Engelhardt, A., Matthijs, H. C., Wittink, F., Bauwe, H., Kaplan, A., &
710 Hagemann, M. (2009). Photorespiratory 2-phosphoglycolate metabolism and

711 photoreduction of O_2 cooperate in high-light acclimation of *Synechocystis* sp. strain PCC
712 6803. *Planta*, *230*(4), 625-637.

713 Helman, Y., Tchernov, D., Reinhold, L., Shibata, M., Ogawa, T., Schwarz, R., ... & Kaplan,
714 A. (2003). Genes encoding A-type flavoproteins are essential for photoreduction of O_2 in
715 cyanobacteria. *Current Biology*, *13*(3), 230-235.

716 Hoffman, B. M., Lukoyanov, D., Yang, Z. Y., Dean, D. R., & Seefeldt, L. C. (2014).
717 Mechanism of nitrogen fixation by nitrogenase: the next stage. Chemical reviews, 114(8),
718 4041-4062.

719 Howe, C., Becker, D., Steinweg, C., Posten, C., & Stensjö, K. (2020). Iron limitation–A
720 perspective on a growth-restricted cultivation strategy for a H2 production system using
721 the diazotrophic cyanobacterium Nostoc PCC 7120 Δ*hupW*. Bioresource Technology
722 Reports, 11, 100508.

723 Huokko, Tuomas, et al. "Role of type 2 NAD (P) H dehydrogenase NdbC in redox
724 regulation of carbon allocation in Synechocystis." Plant physiology 174.3 (2017): 1863-
725 1880.

726 Jiang, Y. L., Wang, X. P., Sun, H., Han, S. J., Li, W. F., Cui, N., ... & Zhou, C. Z. (2018).
727 Coordinating carbon and nitrogen metabolic signaling through the cyanobacterial global
728 repressor NdhR. Proceedings of the National Academy of Sciences, 115(2), 403-408.

729 Jokel, M., Johnson, X., Peltier, G., Aro, E. M., & Allahverdiyeva, Y. (2018). Hunting the
730 main player enabling *Chlamydomonas reinhardtii* growth under fluctuating light. The
731 Plant Journal, 94(5), 822-835.

732 Khetkorn, W., Baebprasert, W., Lindblad, P., & Incharoensakdi, A. (2012). Redirecting the
733 electron flow towards the nitrogenase and bidirectional Hox-hydrogenase by using
734 specific inhibitors results in enhanced H_2 production in the cyanobacterium *Anabaena*
735 siamensis TISTR 8012. *Bioresource technology*, *118*, 265-271.

736 Klähn, S., Orf, I., Schwarz, D., Matthiessen, J. K., Kopka, J., Hess, W. R., & Hagemann,
737 M. (2015). Integrated transcriptomic and metabolomic characterization of the low-carbon
738 response using an *ndhR* mutant of *Synechocystis* sp. PCC 6803. Plant Physiology, 169(3),
739 1540-1556.

740 Kotai, J. (1972). Instructions for preparation of modified nutrient solution Z8 for algae.
741 Norwegian Institute for Water Research, Oslo, 11(69), 5..

742 Latifi, A., Jeanjean, R., Lemeille, S., Havaux, M., & Zhang, C. C. (2005). Iron starvation
743 leads to oxidative stress in Anabaena sp. strain PCC 7120. Journal of Bacteriology,
744 187(18), 6596-6598.

745 Leino, H., Shunmugam, S., Isojärvi, J., Oliveira, P., Mulo, P., Saari, L., ... &
746 Allahverdiyeva, Y. (2014). Characterization of ten H_2 producing cyanobacteria isolated
747 from the Baltic Sea and Finnish lakes. International Journal of Hydrogen Energy, 39(17),
748 8983-8991.

749 Liran, O., Shemesh, E., & Tchernov, D. (2018). Investigation into the CO2 concentrating
750 step rates within the carbon concentrating mechanism of *Synechocystis* sp. PCC6803 at
751 various pH and light intensities reveal novel mechanistic properties. Algal research, 33,
752 419-429.

753 Masukawa, H., Mochimaru, M., & Sakurai, H. (2002). Disruption of the uptake
754 hydrogenase gene, but not of the bidirectional hydrogenase gene, leads to enhanced
755 photobiological hydrogen production by the nitrogen-fixing cyanobacterium Anabaena
756 sp. PCC 7120. *Applied Microbiology and Biotechnology*, *58*(5), 618-624.

757 McDonald, A. E., Amirsadeghi, S., & Vanlerberghe, G. C. (2003). Prokaryotic orthologues
758 of mitochondrial alternative oxidase and plastid terminal oxidase. Plant molecular
759 biology, 53(6), 865-876.

760 Meeks, J. C., & Castenholz, R. W. (1971). Growth and photosynthesis in an extreme
761 thermophile, Synechococcus lividus (Cyanophyta). Archiv für Mikrobiologie, 78(1), 25-
762 41.

763 Mi, H., Endo, T., Ogawa, T., & Asada, K. (1995). Thylakoid membrane-bound, NADPH-
764 specific pyridine nucleotide dehydrogenase complex mediates cyclic electron transport in
765 the cyanobacterium *Synechocystis* sp. PCC 6803. *Plant and Cell Physiology*, *36*(4), 661-
766 668.

767 Mitschke, J., Vioque, A., Haas, F., Hess, W. R., & Muro-Pastor, A. M. (2011). Dynamics
768 of transcriptional start site selection during nitrogen stress-induced cell differentiation in

769 Anabaena sp. PCC7120. Proceedings of the National Academy of Sciences, 108(50),
770 20130-20135.

771 Mustila, H., Paananen, P., Battchikova, N., Santana-Sánchez, A., Muth-Pawlak, D.,
772 Hagemann, M., ... & Allahverdiyeva, Y. (2016). The flavodiiron protein Flv3 functions as
773 a homo-oligomer during stress acclimation and is distinct from the Flv1/Flv3 hetero-
774 oligomer specific to the O2 photoreduction pathway. *Plant and Cell Physiology*, *57*(7),
775 1468-1483.

776 Nawrocki, W. J., Buchert, F., Joliot, P., Rappaport, F., Bailleul, B., & Wollman, F. A.
777 (2019). Chlororespiration controls growth under intermittent light. Plant physiology,
778 179(2), 630-639.

779 Nawrocki, W. J., Tourasse, N. J., Taly, A., Rappaport, F., & Wollman, F. A. (2015). The
780 plastid terminal oxidase: its elusive function points to multiple contributions to plastid
781 physiology. Annual review of plant biology, 66, 49-74.

782 Nikkanen, L., Santana Sánchez, A., Ermakova, M., Rögner, M., Cournac, L., &
783 Allahverdiyeva, Y. (2020). Functional redundancy between flavodiiron proteins and
784 NDH-1 in Synechocystis sp. PCC 6803. *The Plant Journal*, *103*(4), 1460-1476.

785 Picossi, S., Flores, E., & Herrero, A. (2015). The LysR-type transcription factor PacR is a
786 global regulator of photosynthetic carbon assimilation in A nabaena. Environmental
787 microbiology, 17(9), 3341-3351.

788 Robles-Rengel, R., Florencio, F. J., & Muro-Pastor, M. I. (2019). Redox interference in
789 nitrogen status via oxidative stress is mediated by 2-oxoglutarate in cyanobacteria. New
790 Phytologist, 224(1), 216-228.

791 Roumezi, B., Avilan, L., Risoul, V., Brugna, M., Rabouille, S., & Latifi, A. (2020).
792 Overproduction of the Flv3B flavodiiron, enhances the photobiological hydrogen
793 production by the nitrogen-fixing cyanobacterium Nostoc PCC 7120. Microbial cell
794 factories, 19(1), 1-10.

795 Santana-Sanchez, A., Solymosi, D., Mustila, H., Bersanini, L., Aro, E. M., &
796 Allahverdiyeva, Y. (2019). Flavodiiron proteins 1–to-4 function in versatile combinations
797 in O2 photoreduction in cyanobacteria. *Elife*, *8*, e45766.

798 Saroussi, S., Karns, D. A., Thomas, D. C., Bloszies, C., Fiehn, O., Posewitz, M. C., &
799 Grossman, A. R. (2019). Alternative outlets for sustaining photosynthetic electron
800 transport during dark-to-light transitions. Proceedings of the National Academy of
801 Sciences, 116(23), 11518-11527.

802 Shcolnick, S., Summerfield, T. C., Reytman, L., Sherman, L. A., & Keren, N. (2009). The
803 mechanism of iron homeostasis in the unicellular cyanobacterium Synechocystis sp. PCC
804 6803 and its relationship to oxidative stress. Plant Physiology, 150(4), 2045-2056.

805 Sherman, D. M., & Sherman, L. A. (1983). Effect of iron deficiency and iron restoration on
806 ultrastructure of Anacystis nidulans. Journal of bacteriology, 156(1), 393-401.

807 Shi, T., Sun, Y., & Falkowski, P. G. (2007). Effects of iron limitation on the expression of
808 metabolic genes in the marine cyanobacterium Trichodesmium erythraeum IMS101.
809 Environmental Microbiology, 9(12), 2945-2956.

810 Singh, A. K., McIntyre, L. M., & Sherman, L. A. (2003). Microarray analysis of the
811 genome-wide response to iron deficiency and iron reconstitution in the cyanobacterium
812 Synechocystis sp. PCC 6803. Plant physiology, 132(4), 1825-1839.

813 Stepien, P., & Johnson, G. N. (2018). Plastid terminal oxidase requires translocation to the
814 grana stacks to act as a sink for electron transport. Proceedings of the National Academy
815 of Sciences, 115(38), 9634-9639.

816 Storti, M., Puggioni, M. P., Segalla, A., Morosinotto, T., & Alboresi, A. (2020). The
817 chloroplast NADH dehydrogenase-like complex influences the photosynthetic activity of
818 the moss Physcomitrella patens. Journal of Experimental Botany, 71(18), 5538-5548.

819 Storti, M., Segalla, A., Mellon, M., Alboresi, A., & Morosinotto, T. (2020). Regulation of
820 electron transport is essential for photosystem I stability and plant growth. New
821 Phytologist, 228(4), 1316-1326.

822 Tamagnini, P., Leitão, E., Oliveira, P., Ferreira, D., Pinto, F., Harris, D. J., ... & Lindblad,
823 P. (2007). Cyanobacterial hydrogenases: diversity, regulation and applications. *FEMS*
824 *microbiology reviews*, *31*(6), 692-720.

825 Tsygankov, A. A. (2007). Nitrogen-fixing cyanobacteria: a review. *Applied biochemistry*
826 *and microbiology*, *43*(3), 250-259.

827 Vicente, J. B., Gomes, C. M., Wasserfallen, A., & Teixeira, M. (2002). Module fusion in an
828 A-type flavoprotein from the cyanobacterium Synechocystis condenses a multiple-
829 component pathway in a single polypeptide chain. Biochemical and biophysical research
830 communications, 294(1), 82-87.

831 Wang, H. L., Postier, B. L., & Burnap, R. L. (2004). Alterations in global patterns of gene
832 expression in Synechocystis sp. PCC 6803 in response to inorganic carbon limitation and
833 the inactivation of *ndhR*, a LysR family regulator. *Journal of Biological Chemistry*,
834 *279*(7), 5739-5751.

835 Woodger, F. J., Bryant, D. A., & Price, G. D. (2007). Transcriptional regulation of the CO_2-
836 concentrating mechanism in a euryhaline, coastal marine cyanobacterium, *Synechococcus*
837 sp. strain PCC 7002: role of NdhR/CcmR. Journal of Bacteriology, 189(9), 3335-3347.

838 Zhang, C. C., Zhou, C. Z., Burnap, R. L., & Peng, L. (2018). Carbon/nitrogen metabolic
839 balance: lessons from cyanobacteria. *Trends in plant science*, *23*(12), 1116-1130.

840 Zhang, P., Allahverdiyeva, Y., Eisenhut, M., & Aro, E. M. (2009). Flavodiiron proteins in
841 oxygenic photosynthetic organisms: photoprotection of photosystem II by Flv2 and Flv4
842 in *Synechocystis* sp. PCC 6803. *PLoS One*, *4*(4), e533

843

Parsed Citations

Allahverdiyeva, Y., Ermakova, M., Eisenhut, M., Zhang, P., Richaud, P., Hagemann, M., ... & Aro, E. M. (2011). Interplay between flavodiiron proteins and photorespiration in Synechocystis sp. PCC 6803. Journal of Biological Chemistry, 286(27), 24007-24014.
Google Scholar: Author Only Title Only Author and Title

Allahverdiyeva, Y., Mustila, H., Ermakova, M., Bersanini, L., Richaud, P., Ajlani, G., ... & Aro, E. M. (2013). Flavodiiron proteins Flv1 and Flv3 enable cyanobacterial growth and photosynthesis under fluctuating light. Proceedings of the National Academy of Sciences, 110(10), 4111-4116.
Google Scholar: Author Only Title Only Author and Title

Allahverdiyeva, Y., Isojärvi, J., Zhang, P., & Aro, E. M. (2015). Cyanobacterial oxygenic photosynthesis is protected by flavodiiron proteins. Life, 5(1), 716-743.
Google Scholar: Author Only Title Only Author and Title

Bailey, S., Melis, A., Mackey, K. R., Cardol, P., Finazzi, G., van Dijken, G., ... & Grossman, A. (2008). Alternative photosynthetic electron flow to oxygen in marine Synechococcus. Biochimica et Biophysica Acta (BBA)-Bioenergetics, 1777(3), 269-276.
Google Scholar: Author Only Title Only Author and Title

Bolte, S., Marcon, E., Jaunario, M., Moyet, L., Paternostre, M., Kuntz, M., & Krieger-Liszkay, A. (2020). Dynamics of the localization of the plastid terminal oxidase inside the chloroplast. Journal of Experimental Botany, 71(9), 2661-2669.
Google Scholar: Author Only Title Only Author and Title

Bothe, H., Schmitz, O., Yates, M. G., & Newton, W. E. (2010). Nitrogen fixation and hydrogen metabolism in cyanobacteria. Microbiology and molecular biology reviews, 74(4), 529-551.
Google Scholar: Author Only Title Only Author and Title

Braakman, R., Follows, M. J., & Chisholm, S. W. (2017). Metabolic evolution and the self-organization of ecosystems. Proceedings of the National Academy of Sciences, 114(15), E3091-E3100.
Google Scholar: Author Only Title Only Author and Title

Brown, K. A., Guo, Z., Tokmina-Lukaszewska, M., Scott, L. W., Lubner, C. E., Smolinski, S., ... & King, P. W. (2019). The oxygen reduction reaction catalyzed by Synechocystis sp. PCC 6803 flavodiiron proteins. Sustainable Energy & Fuels, 3(11), 3191-3200.
Google Scholar: Author Only Title Only Author and Title

Cai, Y., & Wolk, C. P. (1997). Anabaena sp. strain PCC 7120 responds to nitrogen deprivation with a cascade-like sequence of transcriptional activations. Journal of Bacteriology, 179(1), 267-271.
Google Scholar: Author Only Title Only Author and Title

Chaux, F., Burlacot, A., Mekhalfi, M., Auroy, P., Blangy, S., Richaud, P., & Peltier, G. (2017). Flavodiiron proteins promote fast and transient O2 photoreduction in Chlamydomonas. Plant physiology, 174(3), 1825-1836.
Google Scholar: Author Only Title Only Author and Title

Chen, M., Li, J., Zhang, L., Chang, S., Liu, C., Wang, J., & Li, S. (2014). Auto-flotation of heterocyst enables the efficient production of renewable energy in cyanobacteria. Scientific reports, 4(1), 1-9.
Google Scholar: Author Only Title Only Author and Title

Cumino, A.C., Marcozzi, C., Barreiro, R., & Salerno, G.L. Carbon cycling in Anabaena sp. PCC 7120. Sucrose synthesis in the heterocysts and possible role in nitrogen fixation. Plant Physiology, 143, 1385–1397.
Google Scholar: Author Only Title Only Author and Title

Daley, S. M., Kappell, A. D., Carrick, M. J., & Burnap, R. L. (2012). Regulation of the cyanobacterial CO 2-concentrating mechanism involves internal sensing of NADP+ and α-ketogutarate levels by transcription factor CcmR. PLoS One, 7(7), e41286.
Google Scholar: Author Only Title Only Author and Title

Eisenhut, M., Georg, J., Klähn, S., Sakurai, I., Mustila, H., Zhang, P., ... & Aro, E. M. (2012). The antisense RNA As1_flv4 in the cyanobacterium Synechocystis sp. PCC 6803 prevents premature expression of the flv4-2 operon upon shift in inorganic carbon supply. Journal of Biological Chemistry, 287(40), 33153-33162.
Google Scholar: Author Only Title Only Author and Title

Elanskaya, I. V., Bulychev, A. A., Lukashev, E. P., & Muronets, E. M. (2021). Deficiency in flavodiiron protein Flv3 promotes cyclic electron flow and state transition under high light in the cyanobacterium Synechocystis sp. PCC 6803. Biochimica et Biophysica Acta (BBA)-Bioenergetics, 1862(1), 148318.
Google Scholar: Author Only Title Only Author and Title

Ermakova, M., Battchikova, N., Richaud, P., Leino, H., Kosourov, S., Isojärvi, J., ... & Aro, E. M. (2014). Heterocyst-specific flavodiiron protein Flv3B enables oxic diazotrophic growth of the filamentous cyanobacterium Anabaena sp. PCC 7120. Proceedings of the National Academy of Sciences, 111(30), 11205-11210.
Google Scholar: Author Only Title Only Author and Title

Ermakova, M., Battchikova, N., Allahverdiyeva, Y., & Aro, E. M. (2013). Novel heterocyst-specific flavodiiron proteins in Anabaena sp. PCC 7120. FEBS letters, 587(1), 82-87.

Google Scholar: Author Only Title Only Author and Title

Flaherty, B. L., Van Nieuwerburgh, F., Head, S. R., & Golden, J. W. (2011). Directional RNA deep sequencing sheds new light on the transcriptional response of Anabaena sp. strain PCC 7120 to combined-nitrogen deprivation. BMC genomics, 12(1), 1-10.
Google Scholar: Author Only Title Only Author and Title

Forchhammer, K., & Selim, K. A. (2020). Carbon/nitrogen homeostasis control in cyanobacteria. FEMS microbiology reviews, 44(1), 33-53.
Google Scholar: Author Only Title Only Author and Title

Gerotto, C., Alboresi, A., Meneghesso, A., Jokel, M., Suorsa, M., Aro, E. M., & Morosinotto, T. (2016). Flavodiiron proteins act as safety valve for electrons in Physcomitrella patens. Proceedings of the National Academy of Sciences, 113(43), 12322-12327.
Google Scholar: Author Only Title Only Author and Title

González, A., Bes, M. T., Valladares, A., Peleato, M. L., & Fillat, M. F. (2012). FurA is the master regulator of iron homeostasis and modulates the expression of tetrapyrrole biosynthesis genes in Anabaena sp. PCC 7120. Environmental microbiology, 14(12), 3175-3187.
Google Scholar: Author Only Title Only Author and Title

González, A., Angarica, V. E., Sancho, J., & Fillat, M. F. (2014). The FurA regulon in Anabaena sp. PCC 7120: in silico prediction and experimental validation of novel target genes. Nucleic Acids Research, 42(8), 4833-4846.
Google Scholar: Author Only Title Only Author and Title

Guío, J., Sarasa-Buisan, C., Velázquez-Campoy, A., Bes, M. T., Fillat, M. F., Peleato, M. L., & Sevilla, E. (2020). 2-oxoglutarate modulates the affinity of FurA for the ntcA promoter in Anabaena sp. PCC 7120. FEBS letters, 594(2), 278-289.
Google Scholar: Author Only Title Only Author and Title

Hackenberg, C., Engelhardt, A., Matthijs, H. C., Wittink, F., Bauwe, H., Kaplan, A., & Hagemann, M. (2009). Photorespiratory 2-phosphoglycolate metabolism and photoreduction of O2 cooperate in high-light acclimation of Synechocystis sp. strain PCC 6803. Planta, 230(4), 625-637.
Google Scholar: Author Only Title Only Author and Title

Helman, Y., Tchernov, D., Reinhold, L., Shibata, M., Ogawa, T., Schwarz, R., ... & Kaplan, A. (2003). Genes encoding A-type flavoproteins are essential for photoreduction of O2 in cyanobacteria. Current Biology, 13(3), 230-235.
Google Scholar: Author Only Title Only Author and Title

Hoffman, B. M., Lukoyanov, D., Yang, Z. Y., Dean, D. R., & Seefeldt, L. C. (2014). Mechanism of nitrogen fixation by nitrogenase: the next stage. Chemical reviews, 114(8), 4041-4062.
Google Scholar: Author Only Title Only Author and Title

Howe, C., Becker, D., Steinweg, C., Posten, C., & Stensjö, K. (2020). Iron limitation–A perspective on a growth-restricted cultivation strategy for a H2 production system using the diazotrophic cyanobacterium Nostoc PCC 7120 ΔhupW. Bioresource Technology Reports, 11, 100508.
Google Scholar: Author Only Title Only Author and Title

Huokko, Tuomas, et al. "Role of type 2 NAD (P) H dehydrogenase NdbC in redox regulation of carbon allocation in Synechocystis." Plant physiology 174.3 (2017): 1863-1880.
Google Scholar: Author Only Title Only Author and Title

Jiang, Y. L., Wang, X. P., Sun, H., Han, S. J., Li, W. F., Cui, N., ... & Zhou, C. Z. (2018). Coordinating carbon and nitrogen metabolic signaling through the cyanobacterial global repressor NdhR. Proceedings of the National Academy of Sciences, 115(2), 403-408.
Google Scholar: Author Only Title Only Author and Title

Jokel, M., Johnson, X., Peltier, G., Aro, E. M., & Allahverdiyeva, Y. (2018). Hunting the main player enabling Chlamydomonas reinhardtii growth under fluctuating light. The Plant Journal, 94(5), 822-835.
Google Scholar: Author Only Title Only Author and Title

Khetkorn, W., Baebprasert, W., Lindblad, P., & Incharoensakdi, A. (2012). Redirecting the electron flow towards the nitrogenase and bidirectional Hox-hydrogenase by using specific inhibitors results in enhanced H2 production in the cyanobacterium Anabaena siamensis TISTR 8012. Bioresource technology, 118, 265-271.
Google Scholar: Author Only Title Only Author and Title

Klähn, S., Orf, I., Schwarz, D., Matthiessen, J. K., Kopka, J., Hess, W. R., & Hagemann, M. (2015). Integrated transcriptomic and metabolomic characterization of the low-carbon response using an ndhR mutant of Synechocystis sp. PCC 6803. Plant Physiology, 169(3), 1540-1556.
Google Scholar: Author Only Title Only Author and Title

Kotai, J. (1972). Instructions for preparation of modified nutrient solution Z8 for algae. Norwegian Institute for Water Research, Oslo, 11(69), 5..
Google Scholar: Author Only Title Only Author and Title

Latifi, A., Jeanjean, R., Lemeille, S., Havaux, M., & Zhang, C. C. (2005). Iron starvation leads to oxidative stress in Anabaena sp. strain PCC 7120. Journal of Bacteriology, 187(18), 6596-6598.

Google Scholar: Author Only Title Only Author and Title

Leino, H., Shunmugam, S., Isojärvi, J., Oliveira, P., Mulo, P., Saari, L., ... & Allahverdiyeva, Y. (2014). Characterization of ten H2 producing cyanobacteria isolated from the Baltic Sea and Finnish lakes. International Journal of Hydrogen Energy, 39(17), 8983-8991.
Google Scholar: Author Only Title Only Author and Title

Liran, O., Shemesh, E., & Tchernov, D. (2018). Investigation into the CO2 concentrating step rates within the carbon concentrating mechanism of Synechocystis sp. PCC6803 at various pH and light intensities reveal novel mechanistic properties. Algal research, 33, 419-429.
Google Scholar: Author Only Title Only Author and Title

Masukawa, H., Mochimaru, M., & Sakurai, H. (2002). Disruption of the uptake hydrogenase gene, but not of the bidirectional hydrogenase gene, leads to enhanced photobiological hydrogen production by the nitrogen-fixing cyanobacterium Anabaena sp. PCC 7120. Applied Microbiology and Biotechnology, 58(5), 618-624.
Google Scholar: Author Only Title Only Author and Title

McDonald, A. E., Amirsadeghi, S., & Vanlerberghe, G. C. (2003). Prokaryotic orthologues of mitochondrial alternative oxidase and plastid terminal oxidase. Plant molecular biology, 53(6), 865-876.
Google Scholar: Author Only Title Only Author and Title

Meeks, J. C., & Castenholz, R. W. (1971). Growth and photosynthesis in an extreme thermophile, Synechococcus lividus (Cyanophyta). Archiv für Mikrobiologie, 78(1), 25-41.
Google Scholar: Author Only Title Only Author and Title

Mi, H., Endo, T., Ogawa, T., & Asada, K. (1995). Thylakoid membrane-bound, NADPH-specific pyridine nucleotide dehydrogenase complex mediates cyclic electron transport in the cyanobacterium Synechocystis sp. PCC 6803. Plant and Cell Physiology, 36(4), 661-668.
Google Scholar: Author Only Title Only Author and Title

Mitschke, J., Vioque, A., Haas, F., Hess, W. R., & Muro-Pastor, A. M. (2011). Dynamics of transcriptional start site selection during nitrogen stress-induced cell differentiation in Anabaena sp. PCC7120. Proceedings of the National Academy of Sciences, 108(50), 20130-20135.
Google Scholar: Author Only Title Only Author and Title

Mustila, H., Paananen, P., Battchikova, N., Santana-Sánchez, A., Muth-Pawlak, D., Hagemann, M., ... & Allahverdiyeva, Y. (2016). The flavodiiron protein Flv3 functions as a homo-oligomer during stress acclimation and is distinct from the Flv1/Flv3 hetero-oligomer specific to the O2 photoreduction pathway. Plant and Cell Physiology, 57(7), 1468-1483.
Google Scholar: Author Only Title Only Author and Title

Nawrocki, W. J., Buchert, F., Joliot, P., Rappaport, F., Bailleul, B., & Wollman, F. A. (2019). Chlororespiration controls growth under intermittent light. Plant physiology, 179(2), 630-639.
Google Scholar: Author Only Title Only Author and Title

Nawrocki, W. J., Tourasse, N. J., Taly, A., Rappaport, F., & Wollman, F. A. (2015). The plastid terminal oxidase: its elusive function points to multiple contributions to plastid physiology. Annual review of plant biology, 66, 49-74.
Google Scholar: Author Only Title Only Author and Title

Nikkanen, L., Santana Sánchez, A., Ermakova, M., Rögner, M., Cournac, L., & Allahverdiyeva, Y. (2020). Functional redundancy between flavodiiron proteins and NDH-1 in Synechocystis sp. PCC 6803. The Plant Journal, 103(4), 1460-1476.
Google Scholar: Author Only Title Only Author and Title

Picossi, S., Flores, E., & Herrero, A. (2015). The LysR-type transcription factor PacR is a global regulator of photosynthetic carbon assimilation in Anabaena. Environmental microbiology, 17(9), 3341-3351.
Google Scholar: Author Only Title Only Author and Title

Robles-Rengel, R., Florencio, F. J., & Muro-Pastor, M. I. (2019). Redox interference in nitrogen status via oxidative stress is mediated by 2-oxoglutarate in cyanobacteria. New Phytologist, 224(1), 216-228.
Google Scholar: Author Only Title Only Author and Title

Roumezi, B., Avilan, L., Risoul, V., Brugna, M., Rabouille, S., & Latifi, A. (2020). Overproduction of the Flv3B flavodiiron, enhances the photobiological hydrogen production by the nitrogen-fixing cyanobacterium Nostoc PCC 7120. Microbial cell factories, 19(1), 1-10.
Google Scholar: Author Only Title Only Author and Title

Santana-Sanchez, A., Solymosi, D., Mustila, H., Bersanini, L., Aro, E. M., & Allahverdiyeva, Y. (2019). Flavodiiron proteins 1–to-4 function in versatile combinations in O2 photoreduction in cyanobacteria. Elife, 8, e45766.
Google Scholar: Author Only Title Only Author and Title

Saroussi, S., Karns, D. A., Thomas, D. C., Bloszies, C., Fiehn, O., Posewitz, M. C., & Grossman, A. R. (2019). Alternative outlets for sustaining photosynthetic electron transport during dark-to-light transitions. Proceedings of the National Academy of Sciences, 116(23), 11518-11527.
Google Scholar: Author Only Title Only Author and Title

Shcolnick, S., Summerfield, T. C., Reytman, L., Sherman, L. A., & Keren, N. (2009). The mechanism of iron homeostasis in the unicellular

cyanobacterium Synechocystis sp. PCC 6803 and its relationship to oxidative stress. Plant Physiology, 150(4), 2045-2056.
Google Scholar: Author Only Title Only Author and Title

Sherman, D. M., & Sherman, L. A. (1983). Effect of iron deficiency and iron restoration on ultrastructure of Anacystis nidulans. Journal of bacteriology, 156(1), 393-401.
Google Scholar: Author Only Title Only Author and Title

Shi, T., Sun, Y., & Falkowski, P. G. (2007). Effects of iron limitation on the expression of metabolic genes in the marine cyanobacterium Trichodesmium erythraeum IMS101. Environmental Microbiology, 9(12), 2945-2956.
Google Scholar: Author Only Title Only Author and Title

Singh, A. K., McIntyre, L. M., & Sherman, L. A. (2003). Microarray analysis of the genome-wide response to iron deficiency and iron reconstitution in the cyanobacterium Synechocystis sp. PCC 6803. Plant physiology, 132(4), 1825-1839.
Google Scholar: Author Only Title Only Author and Title

Stepien, P., & Johnson, G. N. (2018). Plastid terminal oxidase requires translocation to the grana stacks to act as a sink for electron transport. Proceedings of the National Academy of Sciences, 115(38), 9634-9639.
Google Scholar: Author Only Title Only Author and Title

Storti, M., Puggioni, M. P., Segalla, A., Morosinotto, T., & Alboresi, A. (2020). The chloroplast NADH dehydrogenase-like complex influences the photosynthetic activity of the moss Physcomitrella patens. Journal of Experimental Botany, 71(18), 5538-5548.
Google Scholar: Author Only Title Only Author and Title

Storti, M., Segalla, A., Mellon, M., Alboresi, A., & Morosinotto, T. (2020). Regulation of electron transport is essential for photosystem I stability and plant growth. New Phytologist, 228(4), 1316-1326.
Google Scholar: Author Only Title Only Author and Title

Tamagnini, P., Leitão, E., Oliveira, P., Ferreira, D., Pinto, F., Harris, D. J., ... & Lindblad, P. (2007). Cyanobacterial hydrogenases: diversity, regulation and applications. FEMS microbiology reviews, 31(6), 692-720.
Google Scholar: Author Only Title Only Author and Title

Tsygankov, A. A. (2007). Nitrogen-fixing cyanobacteria: a review. Applied biochemistry and microbiology, 43(3), 250-259.
Google Scholar: Author Only Title Only Author and Title

Vicente, J. B., Gomes, C. M., Wasserfallen, A., & Teixeira, M. (2002). Module fusion in an A-type flavoprotein from the cyanobacterium Synechocystis condenses a multiple-component pathway in a single polypeptide chain. Biochemical and biophysical research communications, 294(1), 82-87.
Google Scholar: Author Only Title Only Author and Title

Wang, H. L., Postier, B. L., & Burnap, R. L. (2004). Alterations in global patterns of gene expression in Synechocystis sp. PCC 6803 in response to inorganic carbon limitation and the inactivation of ndhR, a LysR family regulator. Journal of Biological Chemistry, 279(7), 5739-5751.
Google Scholar: Author Only Title Only Author and Title

Woodger, F. J., Bryant, D. A., & Price, G. D. (2007). Transcriptional regulation of the CO2-concentrating mechanism in a euryhaline, coastal marine cyanobacterium, Synechococcus sp. strain PCC 7002: role of NdhR/CcmR. Journal of Bacteriology, 189(9), 3335-3347.
Google Scholar: Author Only Title Only Author and Title

Zhang, C. C., Zhou, C. Z., Burnap, R. L., & Peng, L. (2018). Carbon/nitrogen metabolic balance: lessons from cyanobacteria. Trends in plant science, 23(12), 1116-1130.
Google Scholar: Author Only Title Only Author and Title

Zhang, P., Allahverdiyeva, Y., Eisenhut, M., & Aro, E. M. (2009). Flavodiiron proteins in oxygenic photosynthetic organisms: photoprotection of photosystem II by Flv2 and Flv4 in Synechocystis sp. PCC 6803. PLoS One, 4(4), e533
Google Scholar: Author Only Title Only Author and Title